January 30, 2024

Satellite observations reveal positive relationship between trait-based diversity and drought response in temperate forests

Isabelle S. Helfenstein[a*], Joan T. Sturm[a], Bernhard Schmid[a], Alexander Damm[a,b], Meredith C. Schuman[a,c], Felix Morsdorf[a]

[a]Remote Sensing Laboratories, Department of Geography, University of Zurich, Zurich, Switzerland

[b]Eawag, Swiss Federal Institute of Aquatic Science and Technology, Dübendorf, Switzerland

[c]Department of Chemistry, University of Zurich, Zurich, Switzerland

*Corresponding author. Email address: isabelle.helfenstein@geo.uzh.ch

---

KEYWORDS Biodiversity–ecosystem functioning (BEF), functional diversity, plant traits, remote sensing, conservation, ecological monitoring, forest drought response

Abstract

Biodiversity–ecosystem functioning (BEF) relationships are increasingly recognized as an important aspect of ecosystem research and management thanks to knowledge gained from long-term grassland and, more recently, forest experiments. However, to what extent the behavior of non-experimental systems corresponds to the relationships discovered in BEF experiments remains controversial. We investigated the relationship between trait-based diversity and drought response using data from forests in northern Switzerland, which experienced an extremely hot and dry summer in 2018. We used Sentinel-2 satellite data to assess trait diversity and quantified drought response in terms of resistance, recovery, and resilience from 2017 to 2020. We then analyzed the BEF relationship between trait-based diversity and drought response for different aggregation levels of richness and evenness. Forests with greater richness were more resistant and resilient to the drought event, and the relationship of evenness with resistance or resilience was hump-shaped or negative, respectively. These results suggest that trait-based diversity supported forest drought response via a mixture of complementarity and dominance effects, the first indicated by positive richness effects and the second by negative evenness effects. Our results link

ecosystem functioning and biodiversity at large scales and provide new insights into the BEF relationships in real-world forest ecosystems.

1 Introduction

Forests provide habitat for the majority of the world's animal and plant species and are exceptionally rich in biodiversity[1, 2]. Evidence shows that biodiversity positively relates to ecosystem functions (EF) in forests, including productivity[3], carbon storage[4, 5], and water-use efficiency[6]. Furthermore, biodiversity enhances stability, the ability of forests to maintain functioning under stressful environmental conditions[7, 8, 9, 10]. However, biodiversity is in decline worldwide due to human activities and climate change, potentially reducing the capacity of ecosystems to provide valuable services[11]. The protection of biodiversity should be a global priority[12, 13, 14] and is targeted in the UN Sustainable Development Goals for 2030[1].

Rising temperatures due to global change and related evapotranspiration dynamics are predicted to amplify regional drought stress[15] and increasingly challenge the capacity of European forests to maintain high levels of ecosystem functioning, stressing the importance of biodiversity as a mitigating ecosystem property[16]. Ecological drought refers to a deficit in ecosystem water availability below a vulnerability threshold that affects ecosystem services[17]. Drought responses can be divided into resistance — performance during drought, recovery — performance after drought, and resilience — the similarity of the performance before and after the event[18] (Fig. 1). Some studies focusing on forest resistance and resilience found that stands containing multiple species were less affected by drought than mono-specific stands[19, 20], whereas others found no differences in drought responses of trees with different neighboring species[21, 22, 23]. There is growing recognition of the importance of BEF research beyond species richness and considering trait-based diversity to understand the influence of diversity on forest functioning and to demonstrate how trait diversity may promote EF[24, 25, 26]. Rather than the number of species, it is likely the dissimilarity of functions that can positively impact the drought response of forests. This dissimilarity of the functions can be represented by, e.g., morphological traits, such as tree height or wood density[27], or hydraulic traits, such as stem water potential[28].

Trait-based diversity is a widely used approach for quantifying the functional contributions of individuals or species to ecosystem properties[29, 30]. Thus, sampled objects (pixels, individuals, species) can

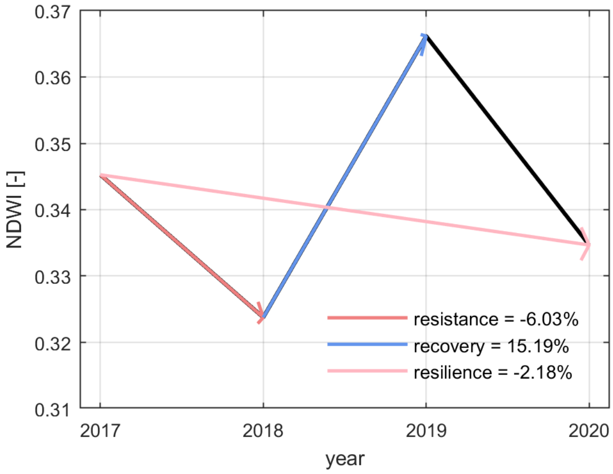

Figure 1: Development of the mean Normalized Difference Water Index (NDWI) in the study area between 2017 and 2020. The numbers in the legend represent the mean percent changes for the three drought-response measures (change 2017 to 2018 resistance, change 2018 to 2019 recovery, change 2017 to 2020 resilience) across the entire study area in northern Switzerland.

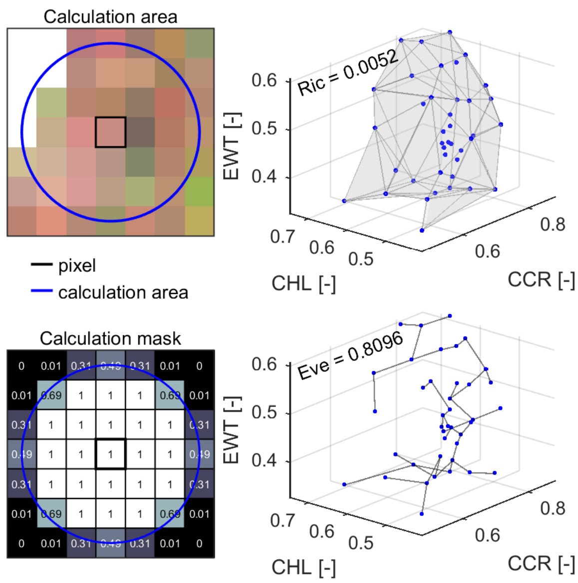

Figure 2: Calculation of diversity metrics from traits within the calculation area (top left). Shown is an example translation of the 60-m radius (blue circle) neighborhood area to a mask for the calculation (bottom left). The numbers indicate the weighting of each pixel in calculating the value of the center pixel. Concepts of diversity metrics (right) in three-dimensional trait space. Richness (Ric) (top right) and evenness (Eve) (bottom right). The three traits considered include chlorophyll content (CHL), carotenoid/chlorophyll ratio (CCR), and equivalent water thickness (EWT).

be classified using traits, defining these objects' functional roles within communities or responses to environmental variables[31, 32]. With increasing functional diversity, a greater range of functional trait values is present, providing opportunities for efficient resource use[33, 34]. Trait-based diversity can be quantified with diversity metrics describing the multidimensional trait space (Fig. 2). We exploit two diversity metrics often used in ecological frameworks: richness and evenness[35]. Richness relates to the hypervolume of the trait space occupied by a community of a certain unit area at a certain time. The larger the resulting value, the greater the extent of the hypervolume, e.g., measured using convex hulls[36, 37]. Evenness measures the regularity of the observations' distribution within the hypervolume[35]. If used with species diversity metrics, evenness refers to similarity of species abundance values independent of species number. Conceptually, evenness reflects how equally available resources in a community are distributed[38]. When the occupation of the hypervolume is skewed toward some specific trait expressions, then those traits are dominant within the community and evenness is low[35]. Conversely, high evenness (i.e., more uniform occupation of the hypervolume) implies weak or no dominance of community members with particular traits[39].

Using remote sensing (RS), trait-based diversity of temperate forest ecosystems may be directly quantified at regional scales, which is particularly relevant because resource management decisions are generally made at these scales[41]. RS complements detailed but local and temporally limited field measurements and provides spatially contiguous and across-scale information on certain traits (e.g., pigments, water content) and their dynamics throughout the phenological cycle[42, 43]. Trait-based diversity is therefore considered an effective measure for mapping biodiversity and detecting its effects on EF from RS data[44, 45, 46, 47].

The sensitivity of satellite-derived trait-based diversity for dynamics in EF in general and the linkage between trait-based diversity and ecosystem drought responses so far has not been rigorously assessed[48, 44, 49]. Filling this gap could advance understanding of climate change impacts on forest ecosystems and pave the way towards large-scale assessment and long-term forest diversity and resilience monitoring. In the present study, we used Sentinel-2-based trait diversity measured at landscape scales in 2017 and Sentinel-2-based drought response assessments from 2017 – 2020 to study the link between trait-based diversity as biodiversity measure and drought response as EF measure for the two cantons Aargau and Zurich on the Swiss Plateau (Fig. 3). We chose this area because abiotic factors (e.g., topography-related

Figure 3: Study area of canton Aargau (west) and canton Zurich (east) and location in Switzerland (top left). Highlighted on the map is the Sihlwald site, where we validated the drought response results. The true color composite shows the study area in summer 2017, based on June/July Sentinel-2 data. The cantonal borders are based on swissBOUNDARIES3D[40].

air temperature and illumination, precipitation) were more or less homogeneous across this area[50], allowing us to focus on relations between variation in tree diversity (mostly management-related) and variations in forest drought response. We compared the changes in canopy water content between pre-drought conditions in 2017, drought conditions in 2018, and post-drought conditions in 2019 and 2020, following the drought response indices proposed by Lloret et al.[18] and adapted by Sturm et al.[50] using Sentinel-2. We focus on how these forest drought responses (resistance, recovery, and resilience) related to trait-based canopy diversity metrics (richness and evenness) from physiological traits. We used three spectral indices as proxies for the physiological canopy traits chlorophyll content (CHL), carotenoid/chlorophyll ratio (CCR), and equivalent water thickness (EWT)[51, 46]. We focused on physiological traits because previous studies have shown that physiological traits are closely linked to drought-sensitive soil variables[46].

Relating functional richness and evenness to species richness and evenness suggests that with high richness, it is possible to have complementarity and selection (i.e., dominance) effects as defined by the additive partitioning method of biodiversity net effects[52]. In a forest with high realized evenness, only complementarity effects can contribute to biodiversity net effects, while dominance effects necessarily reduce realized evenness. At intermediate levels of realized evenness (and high richness), both effects can contribute positively to net biodiversity effects. Therefore, we expected a positive relationship between functional richness and drought response and a hump-backed relationship between evenness and drought response. Furthermore, whereas richness is related to the size of the hypervolume, evenness can be high even within a small hypervolume in trait space, i.e. low richness. Thus, we expected the relationship between functional richness and drought response to be stronger than the relationship between functional evenness and drought response.

2 Results

2.1 Biodiversity data

We calculated diversity maps based on the three canopy traits chlorophyll content (CHL), carotenoid/chlorophyll ratio (CCR), and equivalent water thickness (EWT) (Supplementary Fig. 1, 2). The scatterplot in Fig. 4 shows the distribution of richness and evenness among 21 subregions. The northern regions of the study area had higher richness than the southern regions. Richness was highest in the Rhine plain areas (6, 7, 17, 20, 21), and the lowlands of the Swiss Plateau (2, 13, 16, 19). Areas of lower richness were found towards the south (4, 11, 12). Regarding evenness, areas in the south (1, 3) and southeast (11, 12, 14) showed high values, with the northern regions (5–7, 21) showing lower values. The three Jura regions (8–10), with low richness and evenness values, differ from the rest of the study region.

2.2 Drought-Response Metrics

We derived drought response values across the study area based on the Normalized Difference Water Index (NDWI) data. The entire study area was strongly affected by the drought in 2018, which was visible in a reduction of the NDWI from 2017 to 2018 (see Fig. 1). From 2018 to 2019, the forest of the study area showed an increase in NDWI, followed by a new decrease in 2020 to a level slightly lower than in 2017. Low Resistance values ($< -7.5\%$ in 38.6% of the area, see Supplementary Table 1) occurred in the northern lowlands (Supplementary Fig. 3, top). Most of the forested area (73.5%) showed a $> 7.5\%$ increase in NDWI from 2018 – 2019 (Supplementary Fig. 3, middle). Resilience values $< -7.5\%$ occurred across 28.5% of the area, especially in the southern regions (Supplementary Fig. 3, bottom). We validated the 2020 resilience maps using a classified dataset based on visual interpretation of aerial images (see Sup. 1). Visually damaged areas showed a significantly different drought response than non-damaged areas (Supplementary Fig. 8).

2.3 Relationships between diversity metrics and drought response

We first analyzed the relationship between diversity metrics and drought resistance, recovery, or resilience separately for richness and evenness, grouping these measurements into 1000 bins each. Using the Akaike Information Criterion (AIC) and r2 to determine the optimal model from linear, quadratic, and

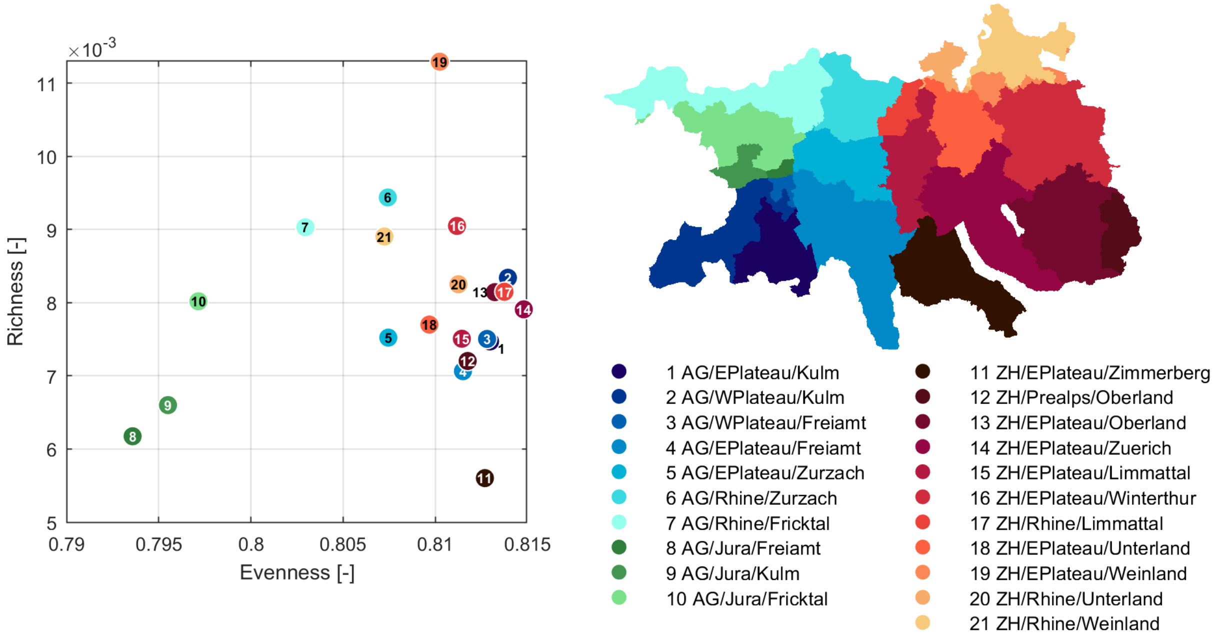

Figure 4: Average diversity of 21 regions with the scatterplot (left) showing their mean richness and evenness. The regions (right) are obtained by grouping the forests of the study area according to the intersection of 1) canton (Aargau (AG) and Zurich (ZH)), 2) biogeographical regions (Central Plateau (Eastern & Western), Rhine plains, Jura, and Pre-Alps), and 3) four, respectively seven, cantonal forest districts. Blue-green colors represent canton AG, and red-yellow colors represent canton ZH. The color gradients range from southern to northern regions within cantons.

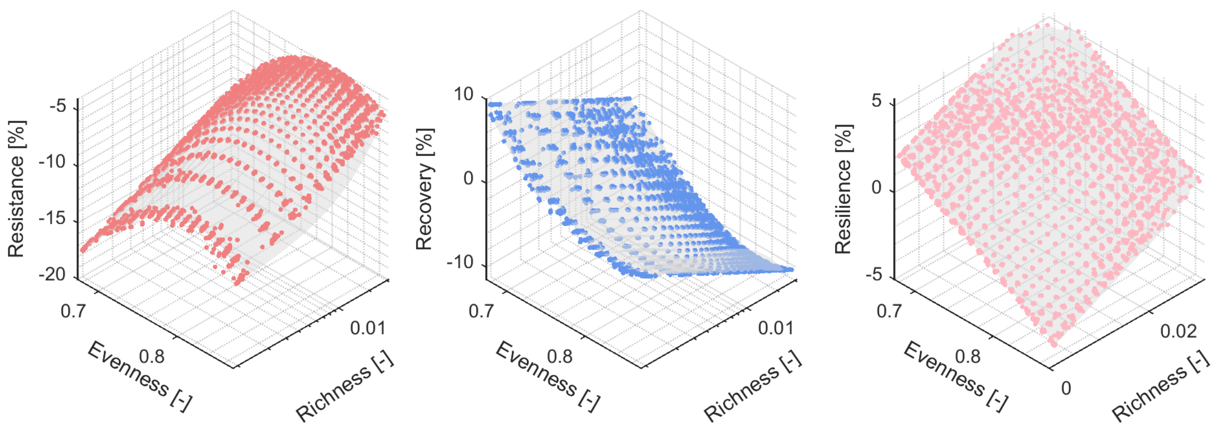

Figure 5: The region-corrected drought-response measures resistance, recovery, and resilience (left to right) as a function of richness and evenness. The data were binned into 20 bins along richness and evenness and into 21 regions, resulting in 8400 bins. We then first fitted region to correct for region differences and then estimated the effects of richness and evenness. Resistance and resilience increased with richness. Resistance showed a hump-backed relationship with evenness, while resilience decreased with evenness.

logarithmic regressions, we found logarithmic relationships between richness and resistance/recovery, while relationships between richness or evenness and resilience were more or less linear (Supplementary Fig. 4). Resistance increased, and recovery decreased with richness at low values of richness and then tempered off whereas resilience generally increased with richness, but with a plateau at intermediate richness levels (Supplementary Fig. 4, top row). Resistance and recovery also increased and decreased, respectively, with evenness at low values of evenness, but at high values, the relationship reversed; resilience generally decreased with increasing evenness (Supplementary Fig. 4, bottom row).

We then analyzed the relationships between richness or evenness and drought responses in combined models, aggregating data using 20 bins each for the two diversity metrics crossed with the 21 regions, yielding a data table with 20 x 20 x 21 = 8400 rows. All bins showed a reduction in NDWI in 2018 (i.e., no bins were fully resistant) and an increase in 2019 (i.e., positive recovery) (Fig. 5).

The best-fitting linear models showed the primary role of richness as a predictor for both resistance and recovery, yet similar roles for richness and evenness as predictor for resilience (Supplementary Tables 2–4). The overall relationships between richness or evenness and drought response were similar when fitted before or after, i.e. corrected for, differences between regions (the latter was used to display the results in Fig. 5). When we compared the BEF relationships between the different geographic regions, significant differences were detected, but these were small compared with the average overall relationship (Supplementary Fig. 6 and Supplementary Tables 2–4). That is, if mean squares for the diversity metrics were compared with mean squares for the corresponding interactions with region, the resulting F-tests were all significant and mostly highly significant (Supplementary Tables 2–4). The regional slopes of resilience as a function of richness and evenness are shown in Supplementary Fig. 7.

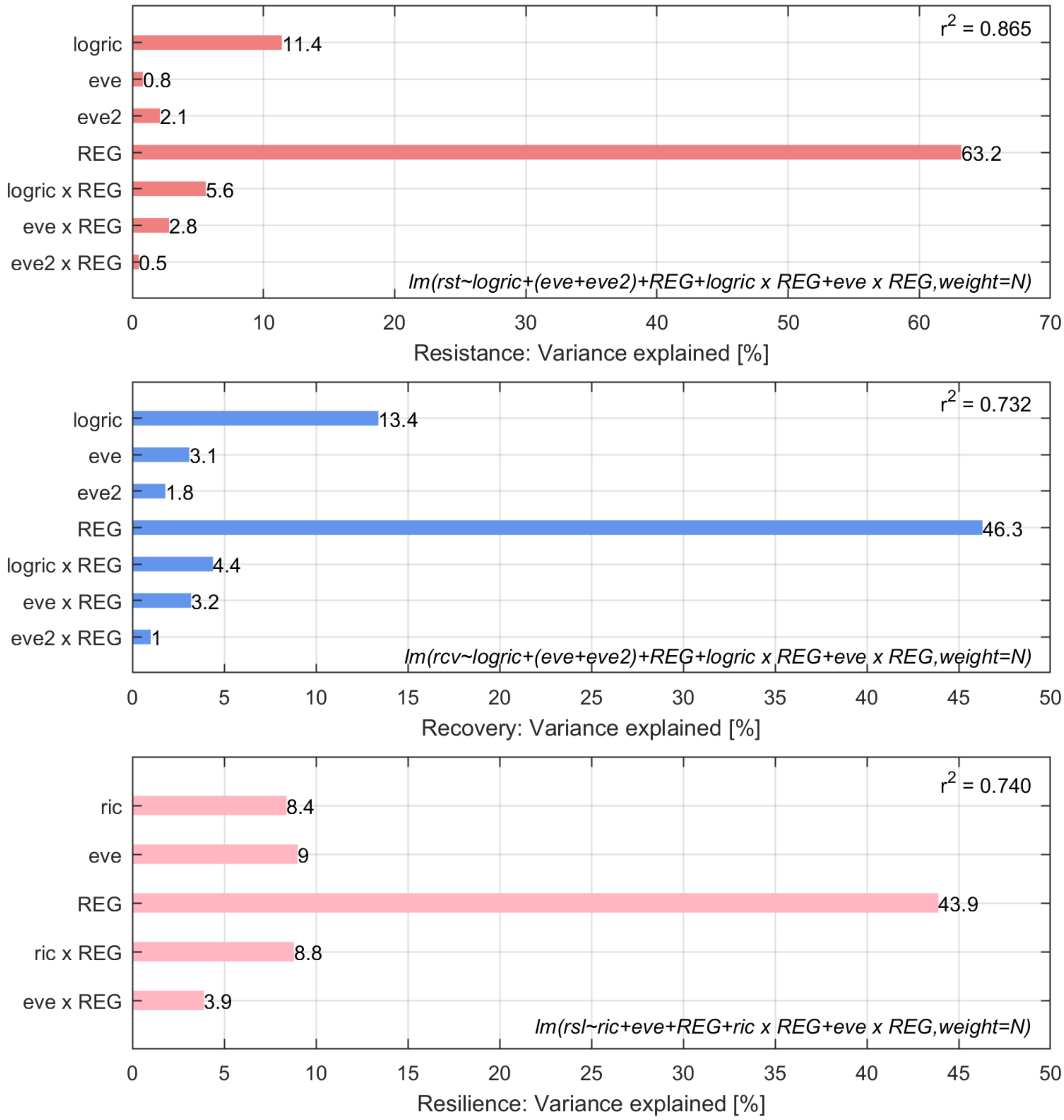

Figure 6: Variance explained by the linear model combining the influence of the diversity metrics richness and evenness on resistance (change in NDWI during the drought 2017 – 2018, Supplementary Table 2), recovery (change in NDWI after the drought 2018 – 2019, Supplementary Table 3) and resilience (change in NDWI after the full two-year observation period 2017 – 2020, Supplementary Table 4). The bars from top to bottom in each panel are the contributions to the r^2 values of linear richness (ric), log-transformed richness (logric), evenness (eve), evenness squared (eve2), the 21 regions (REG), and interactions of the diversity metrics and regions (ric x REG, eve x REG). Note that all contributions are significantly larger than zero. The formulae for the fitted linear models are listed in R[53] notation, with N representing the number of pixels per bin.

3 Discussion

Based on results from plot-scale BEF experiments in grassland and forest ecosystems[54, 55], we hypothesized that more diverse forests from northern Switzerland should have suffered less from an extreme drought event occurring in 2018 across central Europe. We hypothesized a positive relationship between functional richness and drought response and a hump-shaped relationship between functional evenness and drought response. Both hypotheses were broadly supported by our satellite-based dataset. Furthermore, richness effects were generally stronger than evenness effects, again as predicted.

Similar to BEF experiments, drought resistance in our observational study increased linearly with the logarithm of richness across 18 regions, with only three regions showing non-positive relationships. Compensating recovery was negatively related to the logarithm of richness, but resilience was overall linearly increasing with untransformed richness, although five out of the 21 regions showed negative responses. High functional richness likely increases the probability for complementary drought reactions among tree species, thus leading to higher resistance and resilience at the level of entire forest stands. Furthermore, with higher functional richness, it is more likely that a forest stand includes tree species that can contribute strongly to the drought response of the stand and that this will be reflected in uneven abundance distributions among species and thus reduced functional evenness. These two effects resemble complementarity and selection (dominance) effects obtained in additive-partitioning schemes for net biodiversity effects in BEF experiments[56, 57, 52]. In our study, the hump-shaped or negative relationships of functional evenness with drought resistance and resilience, respectively, indicated that a certain level of dominance was beneficial for forest stands of a given functional richness under drought. In our study, these two effects were uncorrelated because evenness was calculated as regularity within a given hypervolume reflecting richness. Thus, evenness could not account for differences in richness and vice versa (see Supplementary Fig. 2). Furthermore, richness and evenness effects were additive, that is, there were no interactive effects of the two on drought responses). Thus, the highest drought resistance was observed in forests with high richness and intermediate levels of evenness, and the highest drought resilience was observed in forests with high richness and low evenness (see Fig. 5). This suggests that a combination of complementarity and dominance effects underpin the relation of forest drought responses with trait-based diversity in the studied temperate forests. Dominant species play a major role in the stability of dry grasslands[58], but how this was related to functional richness and evenness remains unknown. A caveat that remains is that in our study functional unevenness was measured before the extreme drought in 2018 and thus could not be a response to it. However, it is conceivable that forest stands where the earlier, less extreme drought events occurring in 2011 and 2015[59] had led to functional dominance of trees with more resistant and resilient drought responses, compared with other stands, were predisposed to show more resistant and resilient responses to the extreme drought event in 2018.

In contrast to other EF such as production and resistance to disturbances like pest outbreaks[60, 61], evidence about the impact of mixed forests on drought damage so far has been largely lacking[62]. Challenges in understanding the biodiversity–drought resistance relationship may arise from the large scale and low selectivity at which droughts occur, driven by broad climate impacts across extensive forested areas[63]. Because our study was based on functional diversity, we did not directly test to which extent different demographics of species populations contributed to the observed positive functional richness–resistance and –resilience relationships. Although research has explored the direct link between functional traits and drought mortality[64], less is known about trait-based diversity and drought response[65, 63]. Recently, it was found that structural complexity, rather than species diversity alone, explains positive tree richness–productivity relationships in BEF experiments[66]. Furthermore, recent studies point out the importance of functional traits for understanding forest drought response[67].

Regions with low evenness, characterized by high specialization and low competition, may withstand long-term drought effects better, as evidenced by their pronounced recovery[35]. However, drought resilience was negatively related to evenness, meaning that high-evenness regions showed low resilience in 2020. High evenness in a community implies low dominance and high complementarity, promoting efficient resource use through a more regular spacing of trait values. Although high-evenness forests recovered well in 2019, they were severely impacted in 2020 due to resource exhaustion or post-drought disturbances like pests, as competition was found to intensify tree vulnerability during bark beetle outbreaks due to limited resources[68].

High biodiversity, especially species diversity, is suggested to be key to promoting forest resilience to climate change[69, 70], although field-based evidence is still scarce, especially regarding trait-based diversity[71]. Concerning drought resilience in forest ecosystems, functional traits have been demonstrated to play a crucial role in drought response[72, 73]. Furthermore, higher hydraulic diversity was linked to ecosystem resilience, which aligns with our findings[28]. However, our results contrast with previous findings by Espelta et al.[74], where functional dispersion did not relate to the growth response to drought but to mean growth and reduced herbivory[74]. These contrasting findings suggest that the influence of functional diversity may vary depending on the scale of the study, the trait selection, and the characteristics of the forest ecosystem involved. This observation highlights the need for integrating both field-based and remote sensing approaches to obtain a comprehensive understanding of how functional diversity affects forest resilience across various contexts.

We observed a clear dependence between resistance and recovery when stratified for different diversity metrics, i.e., bins with lower resistance in 2018 showed increased recovery in 2019. This compensatory recovery is consistent with previous observations by Sturm et al.[50], who speculated that reduced competition following tree die-back in 2018 may have caused it. Resistance and recovery have also been shown to be negatively related in previous experimental and observational studies[75, 76]. This negative correlation dampens variation in resilience, yet similarities between the resistance and resilience responses to the drought in our studies indicate that the recovery responses could only partly compensate for low resistance. Similar observations have previously been made in diverse forests[28, 27, 67, 50] and suggest that ecosystem stability may generally be more strongly related to resistance than to recovery, with the latter being a "passive partial compensation" of the former. Therefore, we suggest focusing on resistance for predicting stability responses to extreme events such as the 2018 drought year in central Europe.

Many biodiversity studies and related field campaigns focus on either species richness, trait measures per species, or ground-based trait measures, which cannot be directly compared with trait-based canopy diversity as derived from satellite data. There is a need for a systematic evaluation of the links between in-situ measured biodiversity and diversity estimates based on spectral variation[77]. Extensive trait sampling of all species, including non-canopy material and intra-specific differences within the pixel area, would be important to represent the community level as measured by satellites. Trait data sampled using a composite of plots scaled to Sentinel-2 pixels differ from most existing field datasets and would need expensive and prohibitive field effort, especially in forest ecosystems[78]. Validation datasets optimized to capture the spatial, temporal, and species representativeness of satellite data would enable better validation of RS-based trait estimates[79, 80]. Furthermore, additional work is needed to fill the information gap between leaf measurements and satellite data. Trait measurements using close-range RS (e.g., from drones or airborne platforms) might be helpful, as well as upscaling of leaf-level optical properties to canopy spectra using radiative transfer models (RTMs)[81]. Still, the availability of global data indicates applicability to other temperate forest regions, provided that temporal and spatial coverage is sufficient. Trait-based approaches could enable generalization across the forest ecosystems of the world and their highly diverse species compositions[82]. The impact of droughts varies greatly in biomes of different climatic regions[83]. Using the RS-based functional diversity approach presented here, the stability of ecosystems to other disturbances linked to climate change, such as pathogen outbreaks or fires, could also be investigated[44]. Advances in approaches to analyze satellite RS products to map forest disturbances at large scales and analyze patterns in disturbance size, frequency, and severity will support this work[84, 85]. Forest masks needed for this approach can either be derived from governmental maps, as used here, or from LiDAR-derived vegetation height[51]. However, the availability of both data sources is usually geographically limited. Standardized inventories or frameworks for combining Sentinel-2 data and 3D information could support the upscaling of the approach to global applications[86].

Multispectral sensors like Sentinel-2 offer limited spectral bands compared to hyperspectral sensors, reducing the information dimensions available to derive vegetation properties. Imaging spectroscopy expands possibilities for deriving vegetation traits and drought-sensitive indicators, spanning from specific biochemical traits to mapping phylogenetic diversity[87, 88]. Recent spaceborne imaging spectrometers such as EnMAP[89], PRISMA[90], and upcoming missions like CHIME[91] and SBG[92] will advance spaceborne diversity and forest-health monitoring.

There is a need to study EF within the global biodiversity monitoring framework using satellite RS[93]. Many existing datasets show geographic and temporal biases, mainly focusing on temperate ecosystems[94]. Our work builds towards assessing large-scale BEF from satellite data independently of the study area and over time. A major advantage of high-resolution temporal satellite data is repeated and standardized information[95] enabling monitoring of BEF. Results of functional diversity measures and the relationship with drought response might change over time or depending on the season the drought takes place. Monitoring these relationships using satellite data can reveal valuable information for adaptive management.

Insights presented here advance large-scale assessments of the stability and resilience of real-world ecosystems using satellites towards global monitoring of the impacts of biodiversity on EF. Our results indicate that physiological trait-based canopy diversity links to forest drought responses regardless of the species, stand, or extent of sampling. We conclude that increasing drought resistance positively depends on forest richness, while the observed hump-shaped relationship of resistance with evenness suggests an optimum diversity in terms of evenness. We found that drought resilience had a positive relationship with richness and a negative relationship with evenness. Our work explores and confirms the link between trait-based diversity and drought resilience from satellite data, contributes to understanding climate change impacts on forests, and provides the basis for further research on landscape-scale interactions. Derived insights contribute to paving the way toward large-scale assessment and long-term monitoring of forest diversity and BEF using satellite data.

4 Material and Methods

4.1 Study area

The study area comprises the cantons Aargau and Zurich in Switzerland (Fig. 3). Both cantons are located on the northern Central Plateau, subject to different forest management practices, containing different forest types, and providing various ecosystem services[96]. The canton Aargau has a total area of 1403.80 km^2, of which 35% or 490.70 km^2 is forested[97]. The main tree species in canton Aargau are European beech (*Fagus sylvatica*) with 32% of the cantonal stocks, followed by Norway spruce (*Picea abies*) with 26%, silver fir (*Abies alba*) with 14%, and sycamore maple (*Acer pseudoplatanus*) with 5%[98]. The canton of Zurich covers an area of 1728.87 km^2, of which forests cover 29.1% or 503.73 km^2[99]. The main tree species in canton Zurich are *P. abies*, with 35% of the cantonal stocks, *F. sylvatica* with 24%, *A. alba*, with 12%, and ash (*Fraxinus excelsior*) with 8%[100].

We grouped the forests in the study area according to the intersection of cantonal forest districts and biogeographical regions into 21 regions. The subdivision of Switzerland into biogeographical regions of similar ecological characteristics takes account of regional floristic and faunistic conditions[101]. We used the revised biogeographical classification recognized by the Federal Office for the Environment[102, 101]. The study area comprises the biogeographical regions of the eastern and western Plateau, Pre-Alps, Rhine plains, and Jura. Forest districts regulate the territorial authority of the cantonal forest service[103]. The forest-district data were provided by the cantons[103, 104]. Aargau is divided into four and Zurich into seven forestry districts. The intersection of both datasets resulted in 21 regions with forested areas between 3.5 km^2 and 100 km^2.

In 2018 the summer weather in Central Europe was dominated by large precipitation deficits, high temperatures, and sunny conditions over large areas[105]. In Switzerland, the mean precipitation between April and September was just above 500 mm (the lowest since 1962) and the mean temperature was the highest since measurements started in 1864[105]. In the Swiss temperate forests, the drought resulted in early wilting[106], decreased forest health[50], and widespread tree mortality[107]. Secondary drought effects followed; for example, in 2019, the level of wood infested by bark-beetle (*Ips typographus*) reached over one million m^3 for the first time since 2005[107, 108].

Table 1: Acquisition dates (left) and sensor type (Sentinel-2A/B, right) of the satellite data as used for the composites (August 2017 – 2021) to create the drought response maps.

Diversity data		Drought response composite data							
2017				2018		2019		2020	
06-19	2A	08-15	2A	08-03	2A	08-08	2A	07-30	2A
06-26	2A	08-18	2A	08-05	2B	08-18	2A	08-07	2B
07-04	2B	08-23	2B	08-20	2A	08-25	2A	08-09	2A
		08-25	2A	08-23	2A	08-28	2A	08-12	2A
		08-30	2B	08-28	2B	08-30	2B	09-03	2B

4.2 Satellite data

We used a composite of Sentinel-2 data from three dates in June/July 2017 to generate the diversity maps, i.e. Sentinel-2A images from June 19^{th} and 26^{th} and Sentinel-2B data from July 4^{th}. Monthly composites from August in the years 2017 – 2020 were used to assess the drought response (see Table 1). In August, the drought impacts should be at their full strength, whereas the senescence due to the natural phenological cycle is still absent[105, 109]. We ensured the assessments of diversity and drought response were based on independent observations from the independent times of acquisition.

4.3 Satellite data pre-processing

All data were collected using ESA's Scihub and atmospherically corrected using Sen2Cor v.2.9.0. in the ESA Sentinel Application Platform SNAP v9.0. We derived all Sentinel-2 bands available in 10-m or 20-m native spatial resolution. The 10-m bands were resampled to 20 m using mean resampling.

In all images, we flagged all pixels with $< 5\%$ reflectance in band B2 (blue) and $> 15\%$ in band B8A (NIR) as cloud- and cloud-shadow-free, following the approach of Sturm et al.[50]. Additionally, we applied the cantonal polygon forest masks available in LV95 reference system and warped them using gdal to match the projection of the Sentinel-2 data in WGS 84/UTM 32N[110, 111]. To calculate forest traits in June/July 2017, we excluded pixels covering forest gaps, dead canopies, and shadows to tailor the assessment of canopy traits on alive forest canopies only. We therefore derived a forest mask for the scene in June/July 2017, which was then applied to all composites. We set a threshold for the normalized difference vegetation index (NDVI) (bands B4 and B8A) within the forest area. We calculated a median outlier for the forested area, resulting in NDVI thresholds of 0.795 for 06-19, 0.8003 for 06-26, and 0.81 for 07-04. Lastly, we applied shadow masks based on the bands B6 and B12, excluding the darkest pixels in these bands, defined as median outliers from the overall distribution[112]. We calculated three forest maps based on the three acquisitions in June/July 2017. Pixels needed to be valid in two out of three images to be included in the final forest mask using a mean calculation. The resulting forest mask contains 2'293'752 valid pixels and a total forest area of 917.5 km^2.

4.4 Physiological canopy traits

Trait-based diversity from RS can be derived from physiological, morphological, or phenological traits[42, 113]. We focused on physiological traits and related them to forest drought responses since previous studies have shown that physiological traits were closely linked to drought-sensitive soil variables as well as different stages of forest development and local management[46]. Based on the physiological diversity approach initially suggested and applied to APEX imaging spectroscopy data by Schneider et al.[46] and upscaled to Sentinel-2 data by Helfenstein et al.[51], we used three spectral indices as proxies for the physiological canopy traits chlorophyll content (CHL), carotenoid/chlorophyll ratio (CCR), and equivalent water thickness (EWT). All index maps were rescaled to 0 – 1.

CHL was obtained using CIre according to Clevers & Gitelson[114] as

$$CIre = \frac{\rho_{783}}{\rho_{704}} - 1 \tag{1}$$

where ρ stands for the top-of-canopy reflectance at a specific wavelength in nm. We used Sentinel-2 bands B7 and B5. CIre from Sentinel-2 correlated strongly with in-situ measured canopy CHL measured from collected leaves and needles in a mixed mountain forest[115].

As a proxy for CCR, CCI developed for MODIS data and successfully applied to Sentinel-2 data[51] was used. CCI can be calculated according to Gamon[116] as

$$CCI = \frac{\rho_{560} - \rho_{664}}{\rho_{560} + \rho_{664}} \tag{2}$$

We used Sentinel-2 bands B3 and B4 for this calculation.

The Normalized Difference Infrared Index (NDII) was used as proxy for the retrieval of EWT[117, 118, 119]. We used the narrow infrared bands B8A and B11[51, 120] and calculated the NDII according to Hardisky[117].

$$NDII = \frac{\rho_{865} - \rho_{1614}}{\rho_{865} + \rho_{1614}} \tag{3}$$

NDII and NDWI are sometimes synonyms for the same index (e.g., Pan et al.[121]). We here differentiate between NDII and NDWI (see below) using the NIR band 8 for NDWI and band 8A for NDII.

4.5 Diversity metrics and maps

Trait-based diversity measures were derived from the per-pixel trait values using a moving window approach with a circular calculation mask. Based on a previous analysis, we used a three-pixel calculation radius (i.e., 60 m when working with 20-m pixels) to represent the patchy forest in the study area[51]. Fig. 2 shows the calculation and the resulting mask for the moving window. A 60 m radius results in a calculation area of 28.3 pixels or 1.131 ha (Sup. 2 showing the outcome of a multiscale analysis). The calculation radius of 60 m was considered to represent a relatively large ecosystem to landscape scale[122, 123, 47].

We used two components of trait-based diversity (Fig. 2), namely richness and evenness calculated in the multidimensional space spanned by the three traits[35, 37]. Two distinguishable diversity metrics allow a better interpretation of diversity–ecosystem functioning relationships, representing different dimensions of diversity[45, 46] and allow testing of the two hypotheses stated at the end of our Introduction section. Our richness and evenness measures are known to be independent of each other (coefficient of determination of r^2 = 0.001 in our study area).

We calculate richness using concave hulls based on α-shapes around the data points to reduce sensitivity to outliers compared to convex hulls[124, 46, 37]. We complemented the richness of traits with evenness to represent the regularity dimension of the data in the trait space[125, 126]. Evenness was calculated based on the minimum spanning tree (MST) using Euclidean distances between all the points in the trait space[46, 37]. Evenness measures the regularity of the shape of the occupied trait space from the length of the branches in the MST and the evenness in their abundance. The index is derived by normalizing edge weights in the MST and accumulating a sum of minimum partial weighted evenness across vertices, normalized against theoretical minimums[37].

4.6 Drought response maps

Our approach to quantifying drought response in forests is based on Sturm et al.[50]. We calculated the normalized difference water index (NDWI) after Gao[127] using the reflectance in bands B8 NIR and B11 SWIR1 as

$$NDWI = \frac{\rho_{833} - \rho_{1614}}{\rho_{833} + \rho_{1614}} \tag{4}$$

NDWI has been proven sensitive to water stress[128]. The August NDWI values were calculated for each year from 2017 – 2020 by taking the median NDWI value from the images mentioned in Table 1. We assessed the response of forests to the 2018 drought year by comparing the relative pixel-wise percentual change between base NDWI conditions[50] defined from August 2017 and conditions during the drought (2018) or post-drought (2019, 2020) years (Fig. 1). We define resistance as the NDWI change ratio between 2017 and 2018 [$(NDWI_{2018}$-$NDWI_{2017})/NDWI_{2017}$] to assess immediate changes happening during the event, and we define recovery as the change ratio between 2018 and 2019 [$(NDWI_{2019}$-$NDWI_{2018})/NDWI_{2018}$] to assess post-drought changes. Additionally, we define resilience as the change ratio between 2017 and 2020 [$(NDWI_{2020}$-$NDWI_{2017})/NDWI_{2017}$]. We use the second (2020) rather than the first post-drought year (2019) to avoid a linear combination of resilience and recovery[27].

4.7 Separate analysis of drought responses to richness and evenness

Small and isolated patches of forest were excluded from the calculation following Helfenstein et al.[51] because the results of the trait diversity metric were strongly influenced by the number of considered pixels. This step removed 14.35 km^2 or 1.57% of the forest area. We then applied binning to the diversity data to examine the spatial distribution of diversity values. The binning process over the whole study area reduces potential autocorrelation effects, because adjacent pixels with similar values will be combined, and pixels with different values will be separated. We formed 1000 bins of equal range within diversity metrics and averaged drought response values within each bin. Before binning, we conducted image preprocessing by rescaling to a range of 0–1, with the lowest 0.1% set to 0 and the highest 0.1% set to 1. This approach avoided generating empty or small bins that could introduce bias to our subsequent analysis. After the binning process, we excluded bins that contained less than 1% of the maximum pixel number per bin. Richness was divided into 823 bins with values ranging between 0 and 0.261. Evenness was divided into 861 bins with values ranging between 0.6974 and 0.8698. Results without exclusions of bins were very similar and presented in Supplementary Fig. 5. We then used the binned values to investigate the drought responses to richness or evenness in separate linear regression models. The number of pixels per bin were used as weights.

4.8 Combined analysis of drought responses to richness and evenness

We employed linear models to examine the relationships between drought response (resistance, recovery, and resilience) and diversity estimates (richness and evenness), treating the latter as explanatory variables. We discretized the explanatory variables into 20 bins and incorporated 21 geographic regions to account for geographical variation. This resulted in a dataset comprising 8400 strata, calculated as combining 20 richness bins, 20 evenness bins, and 21 geographic regions (Figure 5). Note that this procedure ensures that the three variables richness, evenness, and geographic region are more or less orthogonal to each other, with correlations among them only due to the potential occurrence of empty bins[50].

We directly analyzed the mean NDWI change (resistance and resilience) for each bin while considering forested pixels per bin (N) as a weighting variable. We used the linear models to obtain percentages of total sum of squares (SS) for the different explanatory terms and their interactions in the model (increments of multiple $r^2 * 100$). In all models, we used diversity metrics as continuous variables and geographic region as a 21-level grouping factor. We iteratively refined the models, controlling for region and diversity metrics and interactions. Non-significant explanatory terms ($p \geq .05$) or explanatory terms with SS < 1% were excluded from the models. This procedure resulted in the following linear models for resistance (rst), resistance (rcv), and resilience (rsl), using R notation[53]:

(i) $lm(terms(rst \sim logric + (eve + eve2) + REG + logricxREG + eve2xREG + evexREG,$
$keep.order = T), weight = N)$

(ii) $lm(terms(rcv \sim logric + (eve + eve2) + REG + logricxREG + eve2xREG + evexREG,$
$keep.order = T), weight = N)$

(iii) $lm(terms(rsl \sim ric + eve + REG + ricxREG + evexREG + eve2xREG,$
$keep.order = T), weight = N)$

Here ric = richness, logric = log(richness), eve = evenness, eve2 = evenness squared, REG = region, x = interaction operator, and N = the number of pixels in the bin. We also tested the diversity effects using their interactions with the region as error terms (F2 in Supplementary Tables 2–4). Note that this corresponds to a data analysis using linear mixed models with the interactions as random terms[129]. In the above analyses, richness effects are tested across regions, with the interaction term testing for differences in richness effects between regions. For Fig. 5, richness effects corrected for the region were calculated by fitting the region first in the above linear models. For plotting the thus corrected data, we added the residuals from a linear-model fit with the region as an explanatory term to the overall mean.

5 References

[1] FAO. *The State of the World's Forests 2022. Forest pathways for green recovery and building inclusive, resilient and sustainable economies.* (FAO, Rome, 2022).

[2] Zisenis *et al.* 10 messages for 2010: Forest Ecosystems (2010). URL https://op.europa.eu/en/publication-detail/-/publication/208da612-2517-4c71-9c28-c10cff1937fa/language-en.

[3] Ammer, C. Diversity and forest productivity in a changing climate. *New Phytologist* **221**, 50–66 (2019).

[4] Grossiord, C., Granier, A., Gessler, A., Pollastrini, M. & Bonal, D. The influence of tree species mixture on ecosystem-level carbon accumulation and water use in a mixed boreal plantation. *Forest Ecology and Management* **298**, 82–92 (2013).

[5] Liu, X. *et al.* Tree species richness increases ecosystem carbon storage in subtropical forests. *Proceedings of the Royal Society B* **285**, 20181240 (2018).

[6] Forrester, D. I., Theiveyanathan, S., Collopy, J. J. & Marcar, N. E. Enhanced water use efficiency in a mixed Eucalyptus globulus and Acacia mearnsii plantation. *Forest Ecology and Management* **259**, 1761–1770 (2010).

[7] Craven, D. *et al.* Multiple facets of biodiversity drive the diversity–stability relationship. *Nature Ecology & Evolution* **2**, 1579–1587 (2018).

[8] Isbell, F. *et al.* Biodiversity increases the resistance of ecosystem productivity to climate extremes. *Nature* **526**, 574–577 (2015).

[9] Jucker, T. *et al.* Competition for light and water play contrasting roles in driving diversity–productivity relationships in Iberian forests. *Journal of Ecology* **102**, 1202–1213 (2014).

[10] Schnabel, F. *et al.* Species richness stabilizes productivity via asynchrony and drought-tolerance diversity in a large-scale tree biodiversity experiment. *Science Advances* **7**, eabk1643 (2021).

[11] IPBES. Global assessment report on biodiversity and ecosystem services of the Intergovernmental Science-Policy Platform on Biodiversity and Ecosystem Services. Tech. Rep., IPBES Sectretariat, Bonn, Germany (2019). URL https://ipbes.net/global-assessment.

[12] Mace, G. M. *et al.* Aiming higher to bend the curve of biodiversity loss. *Nature Sustainability* **1**, 448–451 (2018).

[13] Shin, Y. *et al.* Actions to halt biodiversity loss generally benefit the climate. *Global Change Biology* **28**, 2846–2874 (2022).

[14] Wang, L. *et al.* NMDI: A normalized multi-band drought index for monitoring soil and vegetation moisture with satellite remote sensing. *Geophysical Research Letters* **34**, 1011–1019 (2007).

[15] Jacob, D. *et al.* EURO-CORDEX: new high-resolution climate change projections for European impact research. *Regional Environmental Change* **14**, 563–578 (2014).

[16] Ratcliffe, S. *et al.* Biodiversity and ecosystem functioning relations in European forests depend on environmental context. *Ecology Letters* **20**, 1414–1426 (2017).

[17] Crausbay, S. D. *et al.* Defining Ecological Drought for the Twenty-First Century. *Bulletin of the American Meteorological Society* **98**, 2543–2550 (2017).

[18] Lloret, F., Keeling, E. G. & Sala, A. Components of tree resilience: effects of successive low-growth episodes in old ponderosa pine forests. *Oikos* **120**, 1909–1920 (2011).

[19] Lebourgeois, F., Gomez, N., Pinto, P. & Mérian, P. Mixed stands reduce Abies alba tree-ring sensitivity to summer drought in the Vosges mountains, western Europe. *Forest Ecology and Management* **303**, 61–71 (2013).

[20] Pretzsch, H., Schütze, G. & Uhl, E. Resistance of European tree species to drought stress in mixed versus pure forests: evidence of stress release by inter-specific facilitation. *Plant Biology* **15**, 483–495 (2013).

[21] Forrester, D. I. *et al.* Drought responses by individual tree species are not often correlated with tree species diversity in European forests. *Journal of Applied Ecology* **53**, 1725–1734 (2016).

[22] Merlin, M., Perot, T., Perret, S., Korboulewsky, N. & Vallet, P. Effects of stand composition and tree size on resistance and resilience to drought in sessile oak and Scots pine. *Forest Ecology and Management* **339**, 22–33 (2015).

[23] Mölder, I. & Leuschner, C. European beech grows better and is less drought sensitive in mixed than in pure stands: tree neighbourhood effects on radial increment. *Trees* **28**, 777–792 (2014).

[24] Loreau, M. Biodiversity and ecosystem functioning: recent theoretical advances. *Oikos* **91**, 3–17 (2000).

[25] Paquette, A. & Messier, C. The effect of biodiversity on tree productivity: from temperate to boreal forests. *Global Ecology and Biogeography* **20**, 170–180 (2011).

[26] Ruiz-Benito, P. *et al.* Diversity effects on forest carbon storage and productivity. *Global Ecology and Biogeography* **23**, 311–322 (2014).

[27] Gazol, A. & Camarero, J. J. Functional diversity enhances silver fir growth resilience to an extreme drought. *Journal of Ecology* **104**, 1063–1075 (2016).

[28] Anderegg, W. R. L. *et al.* Hydraulic diversity of forests regulates ecosystem resilience during drought. *Nature* **561**, 538–541 (2018).

[29] Bello, F. d. *et al.* Towards an assessment of multiple ecosystem processes and services via functional traits. *Biodiversity and Conservation* **19**, 2873–2893 (2010).

[30] Cadotte, M. W., Carscadden, K. & Mirotchnick, N. Beyond species: Functional diversity and the maintenance of ecological processes and services. *Journal of Applied Ecology* **48**, 1079—1087 (2011).

[31] Cornelissen, J. H. C. *et al.* A handbook of protocols for standardised and easy measurement of plant functional traits worldwide. *Australian Journal of Botany* **51**, 335–380 (2003). URL `internal-pdf://252.28.57.148/Cornelissen-2003-Ahandbookofprotocolsfors.pdf`.

[32] Petchey, O. L. & Gaston, K. J. Functional diversity: Back to basics and looking forward. *Ecology Letters* **9**, 741–758 (2006).

[33] Díaz, S. & Cabido, M. Vive la différence: plant functional diversity matters to ecosystem processes. *Trends in Ecology & Evolution* **16**, 646–655 (2001).

[34] Violle, C. *et al.* Let the concept of trait be functional! *Oikos* **116**, 882–892 (2007).

[35] Mammola, S., Carmona, C. P., Guillerme, T. & Cardoso, P. Concepts and applications in functional diversity. *Functional Ecology* **35**, 1869–1885 (2021).

[36] Cornwell, W. K., Schwilk, D. W. & Ackerly, D. D. A trait-based test for habitat filtering: convex hull volume. *Ecology* **87**, 1465–1471 (2006).

[37] Villéger, S. *et al.* New multidimensional functional diversity indices for a multifaceted framework in functional ecology. *Ecology* **89**, 2290–2301 (2008).

[38] Mason, N. W. H., Mouillot, D., Lee, W. G. & Wilson, J. B. Functional richness, functional evenness and functional divergence: The primary components of functional diversity. *Oikos* **111**, 112–118 (2005).

[39] Perronne, R., Munoz, F., Borgy, B., Reboud, X. & Gaba, S. How to design trait-based analyses of community assembly mechanisms: Insights and guidelines from a literature review. *Perspectives in Plant Ecology, Evolution and Systematics* **25**, 29–44 (2017).

[40] swisstopo. swissBOUNDARIES3D (2021). URL https://www.swisstopo.admin.ch/de/geodata/landscape/boundaries3d.html.

[41] Nelson, E. *et al.* Modeling multiple ecosystem services, biodiversity conservation, commodity production, and tradeoffs at landscape scales. *Frontiers in Ecology and the Environment* **7**, 4–11 (2009).

[42] Homolová, L., Malenovský, Z., Clevers, J. G., García-Santos, G. & Schaepman, M. E. Review of optical-based remote sensing for plant trait mapping. *Ecological Complexity* **15**, 1–16 (2013).

[43] Kokaly, R. F., Asner, G. P., Ollinger, S. V., Martin, M. E. & Wessman, C. A. Characterizing canopy biochemistry from imaging spectroscopy and its application to ecosystem studies. *Remote Sensing of Environment* **113**, S78–S91 (2009).

[44] Jetz, W. *et al.* Monitoring plant functional diversity from space. *Nature Plants* **2**, 1—5 (2016).

[45] Rossi, C. *et al.* From local to regional: Functional diversity in differently managed alpine grasslands. *Remote Sensing of Environment* **236**, 111415 (2020).

[46] Schneider, F. D. *et al.* Mapping functional diversity from remotely sensed morphological and physiological forest traits. *Nature Communications* **8**, 1441 (2017).

[47] Zheng, Z. *et al.* Remotely sensed functional diversity and its association with productivity in a subtropical forest. *Remote Sensing of Environment* **290**, 113530 (2023).

[48] Gamon, J. A. *et al.* Assessing Vegetation Function with Imaging Spectroscopy. *Surveys in Geophysics* **40**, 489–513 (2019).

[49] Schimel, D. S., Asner, G. P. & Moorcroft, P. Observing changing ecological diversity in the Anthropocene. *Frontiers in Ecology and the Environment* **11**, 129–137 (2013).

[50] Sturm, J., Santos, M. J., Schmid, B. & Damm, A. Satellite data reveal differential responses of Swiss forests to unprecedented 2018 drought. *Global Change Biology* **28**, 2956–2978 (2022).

[51] Helfenstein, I. S., Schneider, F. D., Schaepman, M. E. & Morsdorf, F. Assessing biodiversity from space: Impact of spatial and spectral resolution on trait-based functional diversity. *Remote Sensing of Environment* **275**, 113024 (2022).

[52] Loreau, M. *et al.* Ecology: Biodiversity and ecosystem functioning: Current knowledge and future challenges. *Science* **294**, 804–808 (2001).

[53] RStudio. RStudio: Integrated Development Environment for R. (2022). URL www.rstudio.com.

[54] Cardinale, B. J., Ives, A. R. & Inchausti, P. Effects of species diversity on the primary productivity of ecosystems: extending our spatial and temporal scales of inference. *Oikos* **104**, 437–450 (2004).

[55] Schmid, B. *et al.*, Consequences of species loss for ecosystem functioning: meta-analyses of data from biodiversity experiments, *Biodiversity, Ecosystem Functioning, and Human Wellbeing*, 14 – 29, 2009 Oxford University Press.

[56] Fox, J. W. Interpreting the 'selection effect' of biodiversity on ecosystem function. *Ecology Letters* **8**, 846–856 (2005).

[57] Isbell, F. *et al.* Quantifying effects of biodiversity on ecosystem functioning across times and places. *Ecology Letters* **21**, 763–778 (2018).

[58] Wang, Y. *et al.* Stability and asynchrony of local communities but less so diversity increase regional stability of Inner Mongolian grassland. *eLife* **11**, e74881 (2022).

[59] MeteoSchweiz. Klimabulletin Jahr 2019. Tech. Rep., Default Institution, Zurich (2020). URL https://www.meteoswiss.admin.ch/dam/jcr:3f590aa9-4ee0-49ca-882e-1c7b1d3e6bf3/2019_ANN_d.pdf.

[60] Huang, Y. *et al.* Impacts of species richness on productivity in a large-scale subtropical forest experiment. *Science* **362**, 80–83 (2018).

[61] Jactel, H., Moreira, X. & Castagneyrol, B. Tree Diversity and Forest Resistance to Insect Pests: Patterns, Mechanisms and Prospects. *Annual Review of Entomology* **66**, 1–20 (2020).

[62] Bauhus, J. *et al.*, Ecological Stability of Mixed-Species Forests, *Mixed-Species Forests, Ecology and Management*, 2017 337–382.

[63] Jactel, H. *et al.* Tree Diversity Drives Forest Stand Resistance to Natural Disturbances. *Current Forestry Reports* **3**, 223–243 (2017).

[64] O'Brien, M. J. *et al.* A synthesis of tree functional traits related to drought-induced mortality in forests across climatic zones. *Journal of Applied Ecology* **54**, 1669–1686 (2017).

[65] Forrester, D. I. & Bauhus, J. A Review of Processes Behind Diversity—Productivity Relationships in Forests. *Current Forestry Reports* **2**, 45–61 (2016).

[66] Ray, T. *et al.* Tree diversity increases productivity through enhancing structural complexity across mycorrhizal types. *Science Advances* **9**, eadi2362 (2023).

[67] Pardos, M. *et al.* The greater resilience of mixed forests to drought mainly depends on their composition: Analysis along a climate gradient across Europe. *Forest Ecology and Management* **481**, 118687 (2021).

[68] Korolyova, N. *et al.* Primary and secondary host selection by Ips typographus depends on Norway spruce crown characteristics and phenolic-based defenses. *Plant Science* **321**, 111319 (2022).

[69] Messier, C. *et al.* The functional complex network approach to foster forest resilience to global changes. *Forest Ecosystems* **6**, 21 (2019).

[70] Seidl, R. *et al.* Small beetle, large-scale drivers: how regional and landscape factors affect outbreaks of the European spruce bark beetle. *Journal of Applied Ecology* **53**, 530–540 (2016).

[71] Mori, A. S., Lertzman, K. P. & Gustafsson, L. Biodiversity and ecosystem services in forest ecosystems: a research agenda for applied forest ecology. *Journal of Applied Ecology* **54**, 12–27 (2017).

[72] Andrés, E. G. d., Rosas, T., Camarero, J. J. & Martínez-Vilalta, J. The intraspecific variation of functional traits modulates drought resilience of European beech and pubescent oak. *Journal of Ecology* **109**, 3652–3669 (2021).

[73] Powell, T. L. *et al.* Differences in xylem and leaf hydraulic traits explain differences in drought tolerance among mature Amazon rainforest trees. *Global Change Biology* **23**, 4280–4293 (2017).

[74] Espelta, J. M. *et al.* Functional diversity enhances tree growth and reduces herbivory damage in secondary broadleaf forests, but does not influence resilience to drought. *Journal of Applied Ecology* **57**, 2362–2372 (2020).

[75] Gazol, A., Camarero, J. J., Anderegg, W. R. L. & Vicente-Serrano, S. M. Impacts of droughts on the growth resilience of Northern Hemisphere forests. *Global Ecology and Biogeography* **26**, 166–176 (2017).

[76] Wagg, C. *et al.* Plant diversity maintains long-term ecosystem productivity under frequent drought by increasing short-term variation. *Ecology* **98**, 2952–2961 (2017).

[77] Fassnacht, F. E., Müllerová, J., Conti, L., Malavasi, M. & Schmidtlein, S. About the link between biodiversity and spectral variation. *Applied Vegetation Science* **25** (2022).

[78] Hauser, L. T. *et al.* Towards scalable estimation of plant functional diversity from Sentinel-2: In-situ validation in a heterogeneous (semi-)natural landscape. *Remote Sensing of Environment* **262**, 112505 (2021).

[79] Baraloto, C. *et al.* Functional trait variation and sampling strategies in species-rich plant communities. *Functional Ecology* **24**, 208–216 (2010).

[80] Cavender-Bares, J. *et al.* Integrating remote sensing with ecology and evolution to advance biodiversity conservation. *Nature Ecology & Evolution* **6**, 506–519 (2022).

[81] Schneider, F. D. *et al.* Simulating imaging spectrometer data: 3D forest modeling based on LiDAR and in situ data. *Remote Sensing of Environment* **152**, 235–250 (2014).

[82] Kunstler, G. *et al.* Plant functional traits have globally consistent effects on competition. *Nature* **529**, 204–207 (2016).

[83] Liu, Y. *et al.* Assessing the impacts of drought on net primary productivity of global land biomes in different climate zones. *Ecological Indicators* **130**, 108146 (2021).

[84] Hansen, M. C. *et al.* High-Resolution Global Maps of 21st-Century Forest Cover Change. *Science* **342**, 850–853 (2013).

[85] Senf, C. & Seidl, R. Mapping the forest disturbance regimes of Europe. *Nature Sustainability* **4**, 63–70 (2021).

[86] Valbuena, R. *et al.* Standardizing Ecosystem Morphological Traits from 3D Information Sources. *Trends in Ecology & Evolution* **35**, 656–667 (2020).

[87] Czyż, E. A. *et al.* Genetic constraints on temporal variation of airborne reflectance spectra and their uncertainties over a temperate forest. *Remote Sensing of Environment* **284**, 113338 (2023).

[88] Meireles, J. E. *et al.* Leaf reflectance spectra capture the evolutionary history of seed plants. *New Phytologist* **228**, 485–493 (2020).

[89] Guanter, L. *et al.* The EnMAP Spaceborne Imaging Spectroscopy Mission for Earth Observation. *Remote Sensing* **7**, 8830–8857 (2015).

[90] Candela, L. *et al.*, The PRISMA mission, *International Geoscience and Remote Sensing Symposium (IGARSS)*, *2016 IEEE International Geoscience and Remote Sensing Symposium (IGARSS)*, 253–256 (Institute of Electrical and Electronics Engineers Inc., Beijing, China, 2016).

[91] Rast, M., Nieke, J., Adams, J., Isola, C. & Gascon, F. Copernicus Hyperspectral Imaging Mission for the Environment (Chime). *2021 IEEE International Geoscience and Remote Sensing Symposium IGARSS* **00**, 108–111 (2021).

[92] Cawse-Nicholson, K. *et al.* NASA's surface biology and geology designated observable: A perspective on surface imaging algorithms. *Remote Sensing of Environment* **257**, 112349 (2021).

[93] Pettorelli, N. *et al.* Satellite remote sensing of ecosystem functions: opportunities, challenges and way forward. *Remote Sensing in Ecology and Conservation* **4**, 71–93 (2018).

[94] Proença, V. *et al.* Global biodiversity monitoring: From data sources to Essential Biodiversity Variables. *Biological Conservation* **213**, 256–263 (2017).

[95] Pettorelli, N. *et al.* Satellite remote sensing for applied ecologists: opportunities and challenges. *Journal of Applied Ecology* **51**, 839–848 (2014).

[96] Leiterer, R., Furrer, R., Schaepman, M. E. & Morsdorf, F. Retrieval of Canopy Structure Types for Forest Characterization Using Multi-Temporal Airborne Laser Scanning. *2015 IEEE International Geoscience and Remote Sensing Symposium (IGARSS)* 2650–2653 (2015).

[97] Aargau. Aargauer Zahlen 2022. Tech. Rep., Default Institution (2022). URL https://www.ag.ch/media/kanton-aargau/dfr/dokumente/statistik/publikationen/aargauer-zahlen/agz2022-20220513-einzelseiten.pdf.

[98] Aargau. Zustand und Entwicklung des Aargauer Waldes. Ergebnisse der 2. Aargauer Waldinventur 2016. Tech. Rep., Departement Bau, Verkehr und Umwelt, Abteilung Wald, Aarau (2018). URL https://www.ag.ch/media/kanton-aargau/bvu/umwelt-natur/wald/grundlagen/waldinventar/waldinventur-2-150dpi.pdf.

[99] Zürich. Statistisches Jahrbuch des Kantons Zürich 2020. Tech. Rep., Default Institution (2020). URL https://www.zh.ch/content/dam/zhweb/bilder-dokumente/themen/bildung/bildungssystem/zahlen/statistisches_jahrbuch_kanton_zuerich_2020.pdf.

[100] Zürich. Zwischenbericht Waldentwicklung 2020. Tech. Rep., Default Institution (2020). URL www.zh.ch/wald.

[101] BAFU. Die biogeografischen Regionen der Schweiz. 1. aktualisierte Auflage 2022. Erstausgabe 2001. *Bundesamt für Umwelt, Bern. Umwelt-Wissen* **2214**, 28 (2022).

[102] BAFU. Biogeographische Regionen der Schweiz (CH) (2004). URL https://opendata.swiss/de/dataset/biogeographische-regionen-der-schweiz-ch.

[103] AGIS. 76-AG Forstkreise und Forstreviere (2023). URL https://www.ag.ch/geoportal/geodatenshop/Datendokumentation.aspx?Datensatzelement=5382.

[104] GIS-ZH. Forstkreise (OGD) (2019). URL https://geolion.zh.ch/geodatensatz/show?giszhnr=226.

[105] MeteoSchweiz. Hitze und Trockenheit im Sommerhalbjahr 2018 - eine klimatologische Übersicht. Tech. Rep., Default Institution (2018).

[106] Brun, P. *et al.* Large-scale early-wilting response of Central European forests to the 2018 extreme drought. *Global Change Biology* **26**, 7021–7035 (2020).

[107] Schuldt, B. *et al.* A first assessment of the impact of the extreme 2018 summer drought on Central European forests. *Basic and Applied Ecology* **45**, 86–103 (2020).

[108] Stroheker, S., Forster, B. & Queloz, V. Zweithöchster je registrierter Buchdruckerbefall (Ips typographus) in der Schweiz. *Waldschutz aktuell* **1/2020**, 2 (2020).

[109] Zubler, E. M., Scherrer, S. C., Croci-Maspoli, M., Liniger, M. A. & Appenzeller, C. Key climate indices in Switzerland; expected changes in a future climate. *Climatic Change* **123**, 255–271 (2014).

[110] AGIS. Waldareal (2019). URL https://www.ag.ch/geoportal/geodatenshop/Datendokumentation.aspx?Datensatzelement=5464.

[111] GIS-ZH. Waldareal (OGD) (2019). URL https://www.geolion.zh.ch/geodatenservice/show?nbid=1257.

[112] Rüfenacht, D. *et al.* Automatic and accurate shadow detection using near-infrared information. *IEEE Transactions on Pattern Analysis and Machine Intelligence* **36**, 1672–1678 (2014).

[113] Kattge, J. *et al.* TRY - a global database of plant traits. *Global Change Biology* **17**, 2905–2935 (2011).

[114] Clevers, J. G. P. W. & Gitelson, A. A. Remote estimation of crop and grass chlorophyll and nitrogen content using red-edge bands on Sentinel-2 and -3. *International Journal of Applied Earth Observation and Geoinformation* **23**, 344–351 (2013).

[115] Ali, A. M. *et al.* Comparing methods for mapping canopy chlorophyll content in a mixed mountain forest using Sentinel-2 data. *International Journal of Applied Earth Observation and Geoinformation* **87**, 102037 (2020).

[116] Gamon, J. A. *et al.* A remotely sensed pigment index reveals photosynthetic phenology in evergreen conifers. *Proceedings of the National Academy of Sciences of the United States of America* **113**, 13087–13092 (2016).

[117] Hardisky, M. A., Klemas, V. & Smart, R. M. The Influence of Soil Salinity, Growth Form, and Leaf Moisture on-the Spectral Radiance of Spartina alterniflora Canopies. *Photogrammetric ENgineering and Remote Sensing* **49**, 77–83 (1983).

[118] Wilson, N. R. & Norman, L. M. Analysis of vegetation recovery surrounding a restored wetland using the normalized difference infrared index (NDII) and normalized difference vegetation index (NDVI). *International Journal of Remote Sensing* **39**, 3243–3274 (2018).

[119] Yilmaz, M. T., Hunt, E. R. & Jackson, T. J. Remote sensing of vegetation water content from equivalent water thickness using satellite imagery. *Remote Sensing of Environment* **112**, 2514–2522 (2008).

[120] Hill & Michael, J. Vegetation index suites as indicators of vegetation state in grassland and savanna: An analysis with simulated SENTINEL 2 data for a North American transect. *Remote Sensing of Environment* **137**, 94–111 (2013).

[121] Pan, H., Chen, Z., Ren, J., Li, H. & Wu, S. Modeling Winter Wheat Leaf Area Index and Canopy Water Content With Three Different Approaches Using Sentinel-2 Multispectral Instrument Data. *IEEE Journal of Selected Topics in Applied Earth Observations and Remote Sensing* **12**, 482–492 (2018).

[122] Oehri, J., Schmid, B., Schaepman-Strub, G. & Niklaus, P. A. Terrestrial land-cover type richness is positively linked to landscape-level functioning. *Nature Communications* **11**, 1–10 (2020).

[123] Zhang, H. *et al.* Using functional trait diversity patterns to disentangle the scale-dependent ecological processes in a subtropical forest. *Functional Ecology* **32**, 1379–1389 (2018).

[124] Gruson, H. Estimation of colour volumes as concave hypervolumes using α-shapes. *Methods in Ecology and Evolution* **11**, 955–963 (2020).

[125] Mouillot, D. *et al.* Functional over-redundancy and high functional vulnerability in global fish faunas on tropical reefs. *Proceedings of the National Academy of Sciences* **111**, 13757–13762 (2014).

[126] Schleuter, D., Daufresne, M., Massol, F. & Argillier, C. A user's guide to functional diversity indices. *Ecological Monographs* **80**, 469–484 (2010).

[127] Gao, B.-c. NDWI - A normalized difference water index for remote sensing of vegetation liquid water from space. *Remote Sensing of Environment* **58**, 257—266 (1996). URL http://linkinghub.elsevier.com/retrieve/pii/S0034425796000673.

[128] Marusig, D. *et al.* Correlation of Field-Measured and Remotely Sensed Plant Water Status as a Tool to Monitor the Risk of Drought-Induced Forest Decline. *Forests* **11**, 77 (2020).

[129] Schmid, B., Baruffol, M., Wang, Z. & Niklaus, P. A. A guide to analyzing biodiversity experiments. *Journal Of Plant Ecology* **10**, 91–110 (2017).

6 Acknowledgements

This research project and related results were made possible with the support of the NOMIS Foundation and the University Research Priority Program on Global Change and Biodiversity of the University of Zurich. The authors thank the cantons Aargau and Zurich for valuable forest and RS data and the Nature Reserve Sihlwald for valuable discussions.

Supplementary Material

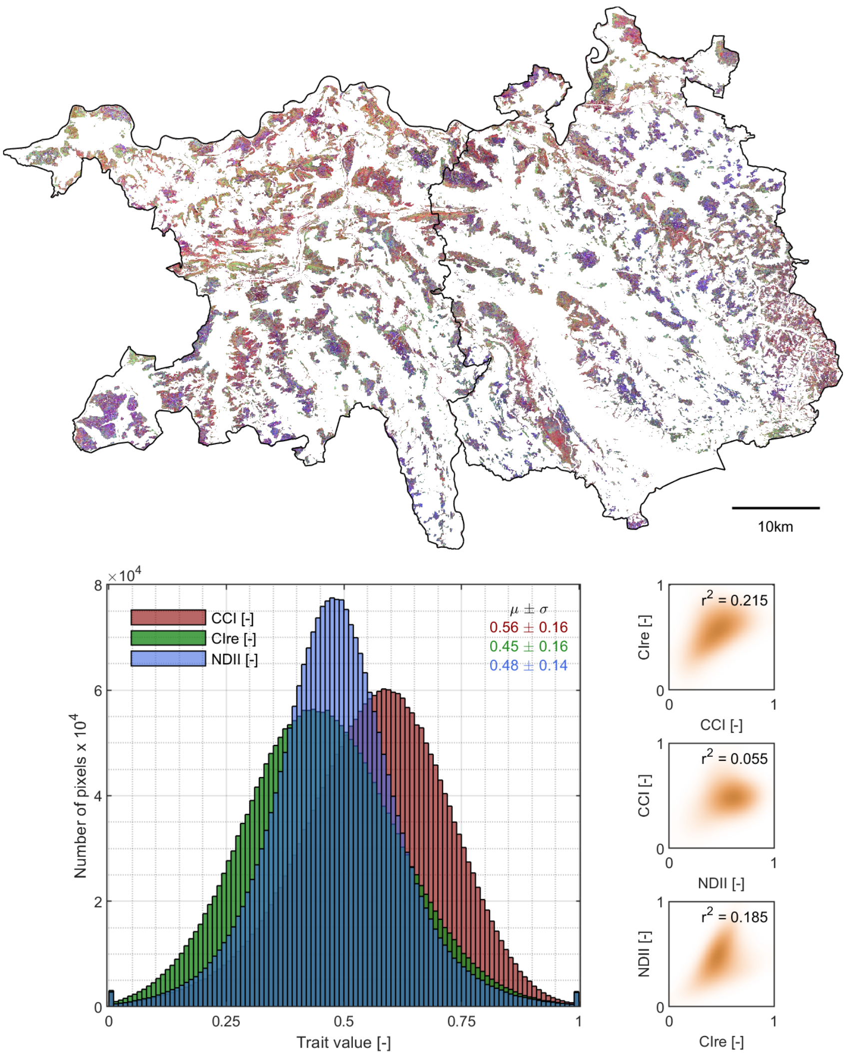

Supplementary Figure S1: Top: calculated indices CIre (green), CCI (red), and NDII (blue) as proxies for the physiological traits CHL, CCR, and EWT at the research site and normalized between 0 and 1. Bottom left: histogram of physiological traits, including means and standard deviations. Bottom right: coefficient of determination of vegetation indices. CIre and CCI show the highest coefficient of determination with $r^2 = 0.215$, followed by CIre and NDII with $r^2 = 0.185$ and CCI and NDII with $r^2 = 0.055$.

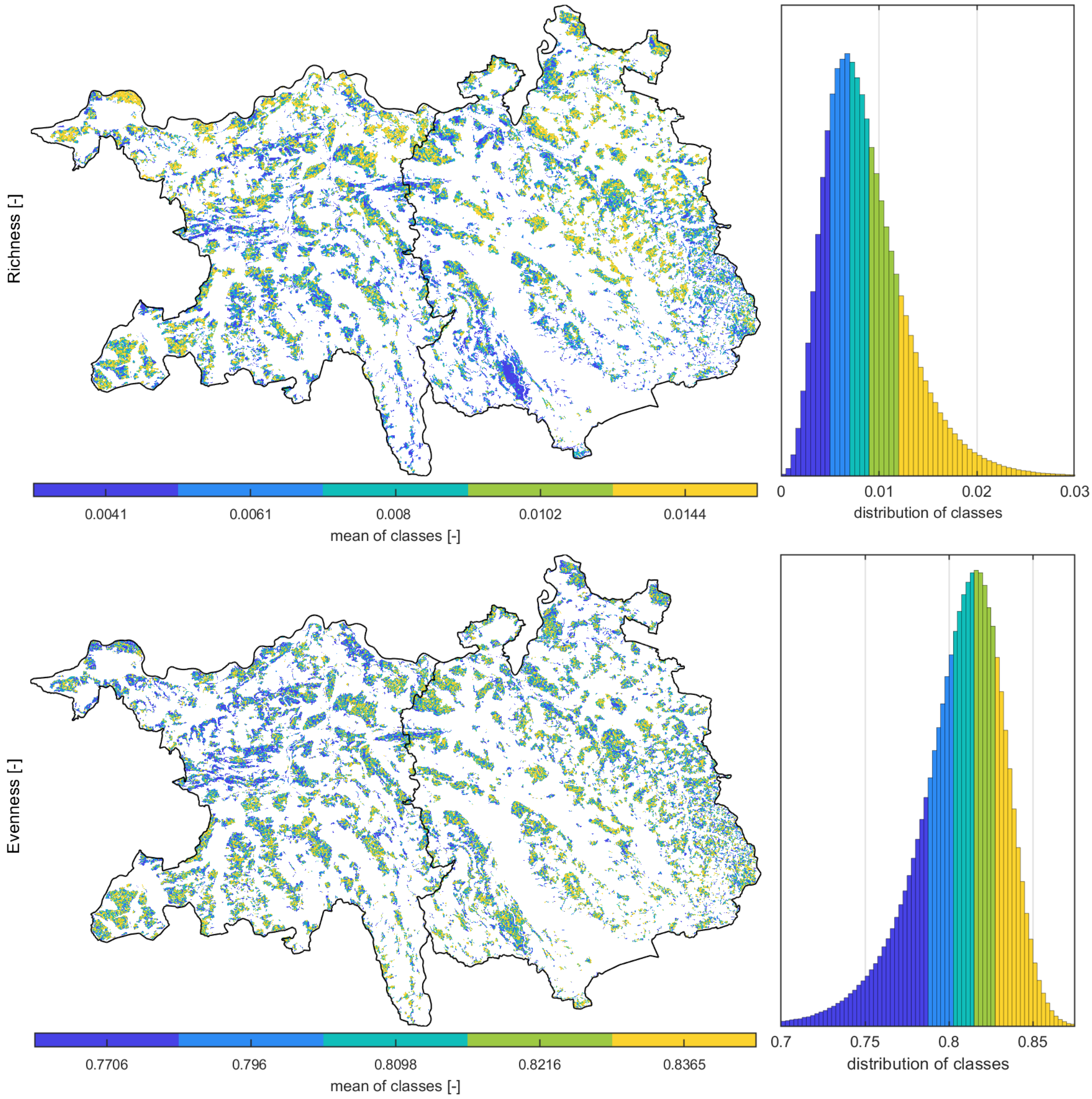

Supplementary Figure S2: Functional richness and functional evenness maps of the study area (left) and histograms of distribution (right) calculated at a 60 m radius. The histogram colors indicate 20%-percentiles, with the mean of every class in the color bars. The histogram of richness is slightly skewed toward zero, and richness varies between zero and 0.03. Evenness varies between 0.7 and 0.9, with a histogram skewed towards 1. The richness and evenness map showed a correlation coefficient of r = 0.027.

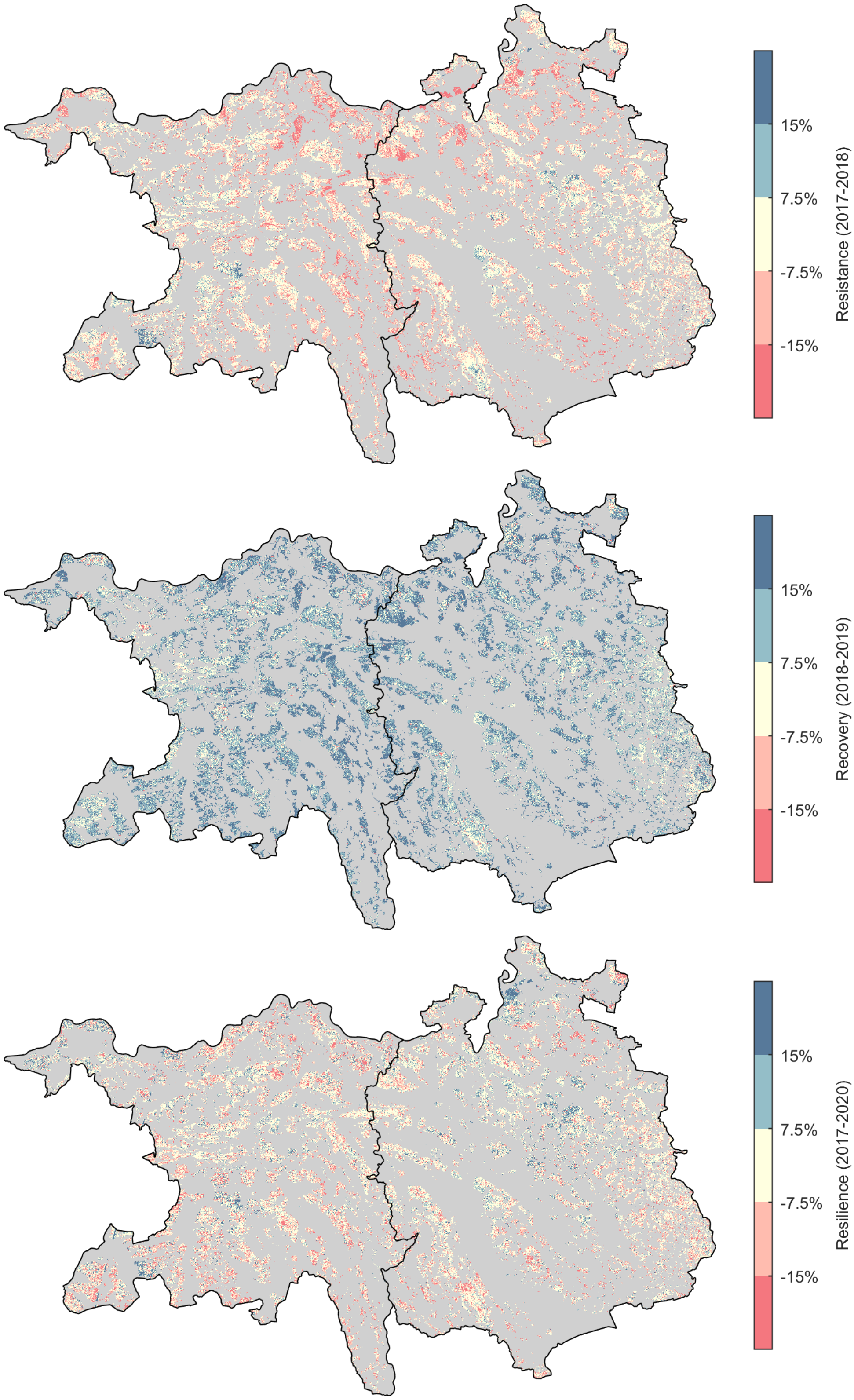

Supplementary Figure S3: Drought response of forest ecosystems. NDWI-based drought response for the forested area in August composites for 2017–2020. The drought response is quantified using resistance (top, difference 2017–2018 in percent of 2017), recovery (center, difference 2018–2019 in percent of 2018), and resilience (bottom, difference 2017–2020 in percent of 2017). The mean resistance was -6.03%, mean recovery was 15.19% and resilience was -2.18%.

Supplementary Table S1: Area of forest response strength to the drought of 2018. Resistance, recovery, and resilience were divided into five classes, from strongly negative ($< -15\%$) to strongly positive ($> 15\%$) changes of the Normalized Difference Water Index (NDWI). The percentage of forest area falling into each class for each drought response measure is indicated.

Change	$< -15\%$	$< -7.5\%$	$-7.5\% - 7.5\%$	$> 7.5\%$	$> 15\%$	Total
Resistance	16.15%	22.47%	53.80%	5.53%	2.05%	100%
Recovery	1.50%	1.37%	23.62%	33.13%	40.38%	100%
Resilience	12.15%	16.34%	54.05%	10.92%	6.53%	100%

Supplementary Table S2: Analysis of variance for resistance as dependent variable and diversity metrics and region as explanatory terms. logric = log-transformed richness, eve = evenness, eve2 = evenness squared, REG = region, Df = degree of freedom, SS = sum of squares (in thousands), %SS = SS in percent (corresponding to increments of model multiple r2 * 100), MS = mean square, F1 = F-ratio using MS of residuals as denominator, F2 = F-ratio using MS of interaction with region as denominator (this corresponds to a mixed-model analysis with the interaction as random-effects term). All F1 were highly significant (p <0.001), for F2 significances are indicated by asterisks (*** p <0.001, * p <0.05).

Response:	rst					
	Df	SS/1000	%SS	MS/1000	F1	F2
logric	1	2744	11.38	2744	5237	40.6***
eve	1	201	0.83	201	384.5	5.9*
eve2	1	509	2.11	509	970.7	85.9***
REG	20	15240	63.22	762	1454.4	
logric x REG	20	1352	5.61	68	129.1	
eve x REG	20	678	2.81	34	64.7	
eve2 x REG	20	119	0.49	6	11.30	
Residuals	6232	3265	13.54	0.5		
Total	6315	24108	100			
		r^2	0.865			

Supplementary Table S3: Analysis of variance for recovery as dependent variable and diversity metrics and region as explanatory terms. logric = log-transformed richness, eve = evenness, eve2 = evenness squared, REG = region, Df = degree of freedom, SS = sum of squares (in thousands), %SS = SS in percent (corresponding to increments of model multiple r2 * 100), MS = mean square, F1 = F-ratio using MS of residuals as denominator, F2 = F-ratio using MS of interaction with region as denominator (this corresponds to a mixed-model analysis with the interaction as random-effects term). All F1 were highly significant (p <0.001), for F2 significances are indicated by asterisks (*** p <0.001).

Response:	rcv					
	Df	SS/1000	%SS	MS/1000	F1	F2
logric	1	5331	13.40	5331	3119.8	61.2***
eve	1	1251	3.14	1251	732.1	19.5***
eve2	1	724	1.82	724	423.8	37.5***
REG	20	18421	46.30	921	539	
logric x REG	20	1744	4.38	87	51	
eve x REG	20	1284	3.23	64	37.6	
eve2 x REG	20	385	0.97	19	11.3	
Residuals	6232	10650	26.77	1.7		
Total	6315	39790	100			
		r^2	0.732			

Supplementary Table S4: Analysis of variance for resilience as dependent variable and diversity metrics and region as explanatory terms. ric = richness, eve = evenness, eve2 = evenness squared, REG = region, Df = degree of freedom, SS = sum of squares (in thousands), %SS = SS in percent (corresponding to increments of model multiple r2 * 100), MS = mean square, F1 = F-ratio using MS of residuals as denominator, F2 = F-ratio using MS of interaction with region as denominator (this corresponds to a mixed-model analysis with the interaction as random-effects term). All F1 were highly significant (p <0.001), for F2 significances are indicated by asterisks (*** p <0.001).

Response:	rsl					
	Df	SS/1000	%SS	MS/1000	F1	F2
ric	1	1582	8.43	1582	2027.8	19.2***
eve	1	1692	9.01	1692	2168.8	45.9***
REG	20	8239	43.89	412	528.2	
ric x REG	20	1647	8.77	82	105.6	
eve x REG	20	737	3.93	37	47.2	
Residuals	6253	4877	25.98	0.8		
Total	6315	18774	100			
		r^2	0.740			

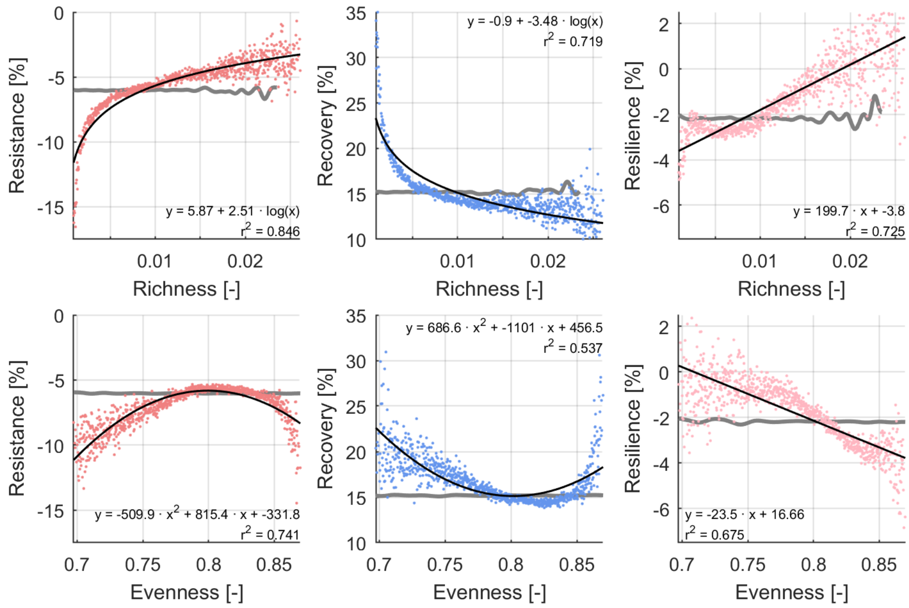

Supplementary Figure S4: Resistance, recovery, and resilience (left to right) binned to 1000 bins of richness (top) and evenness (bottom) calculated at a 60 m radius. The black line represents the best-fit function. The gray line shows the null model of the experiment (all trait values shuffled prior to the calculation).

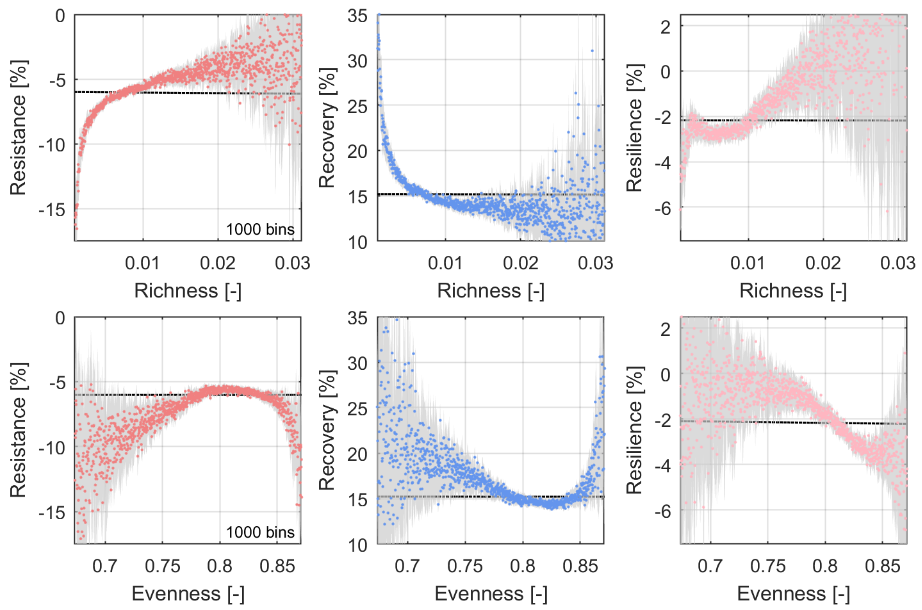

Supplementary Figure S5: Resistance, recovery, and resilience (left to right) binned to 1000 bins of functional richness (top) and functional evenness (bottom) calculated at a 60 m radius. Empty or small bins are included in the graph, showing high variability within the bins. The gray area represents the 99% confidence interval.

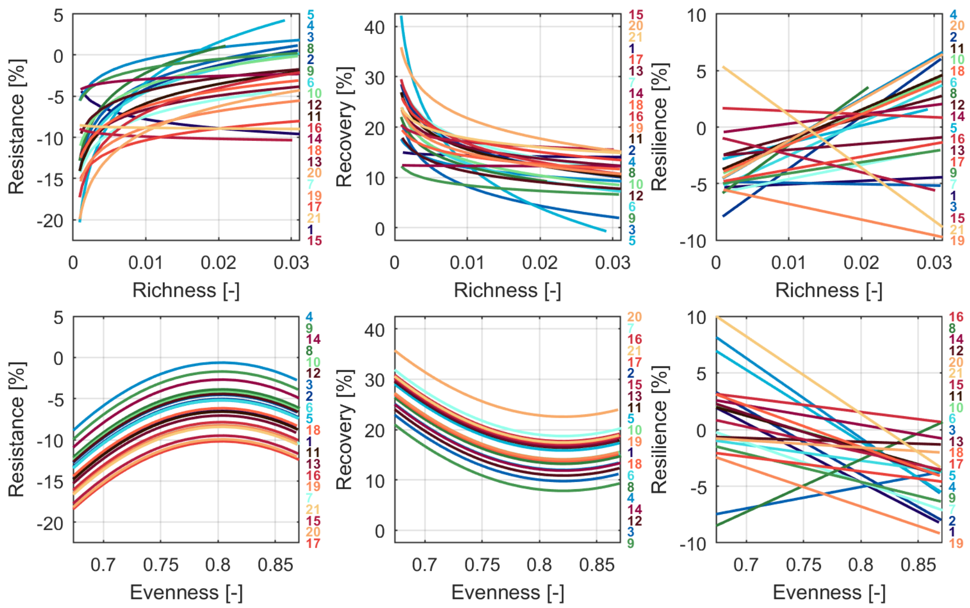

Supplementary Figure S6: Regional drought responses resistance, recovery and resilience (left to right) as functions of functional richness (top) and functional evenness (bottom) calculated at a 60 m radius.

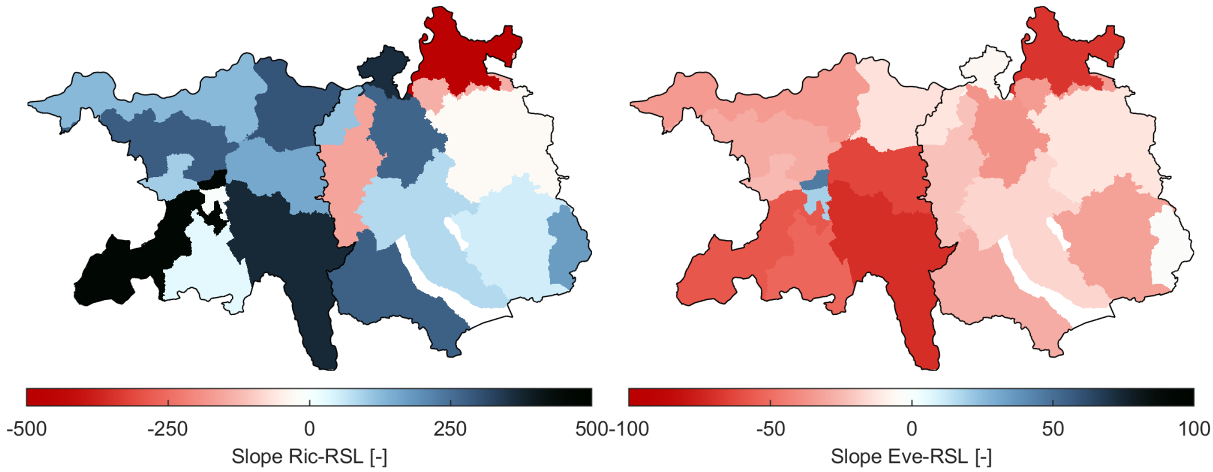

Supplementary Figure S7: Regional slopes of resilience (RSL) as a function of functional richness (Ric) (left) and functional evenness (Eve) (right). Blue colors represent increasing slopes, red colors represent decreasing slopes.

1 Validation of the drought resilience maps

To validate the 2020 resilience approach, we prepared a reference dataset with 271 data points representing 20-m Sentinel-2 pixels for the Sihlwald region. The Sihlwald is a 1098-ha natural reserve, ranging from 483 to 866 m a.s.l. in the southeast of the study area [1]. Each 20-m pixel was optically evaluated for damage in the canopy and classified as damaged or intact in 2020 and unharmed in 2018.

Sihlwald reported damage without any management cuttings, which excludes potential bias due to the removal of damaged trees with the potential to recover in the seasons between 2018 and 2020. The only exception is around pathways and roads to minimize the risk of falling trees for visitors and traffic. The park data were based on the forest inventory from 1990 (GIS Wildnispark Zürich & Grün Stadt Zürich, [2]).

We created the validation dataset using aerial images RGB/infrared from summer 2018/2020 provided by the canton of Zurich [3, 4]. The 2018 dataset was acquired in the Sihlwald area between 27 July 2018 and 3 August 2018 on two dates. The 2020 data were acquired on three days between 9 and 12 August 2020. Both images were resampled to 0.5 m. Using high-resolution optical data gave clear advantages over identifying crown damage in the field. Data digitized by the canton allowed us to locate the pixels containing the canopy unambiguously, and we could see damage to the top layer of the forest, which might not necessarily have been visible from the ground in the forest.

We labeled intact and damaged satellite pixels by interpreting a pre-selection through high-resolution images of the area of interest. An example of this method is shown in Supplementary Figure S8. The pre-selection was done by calculating the mean μ and standard deviation σ of the change in NDVI for the pixels that showed NDVI values of > 0.4 in 2018. Satellite pixels needed a minimum of 75% healthy forest pixels in 2018. Pixels showing a negative change of $< 2\sigma$ from the mean change were pre-classified as 'damaged,' and pixels showing a positive, neutral, or negative change $> \sigma$ from the mean change in NDVI were classified as 'intact.' We ended up with a pre-selection of 649 damaged and 2834 intact pixels. We selected the pixels in a random sampling for optical selection of the validation dataset from 200 pixels per class, regularly distributed along the test site. We optically decided if the canopy showed significant ($> 50\%$ of the pixel area) damage to the canopy in 2020 or was optically intact and healthy. The criteria to be selected for the reference were an intact canopy in 2018 and, if visible, no roads in

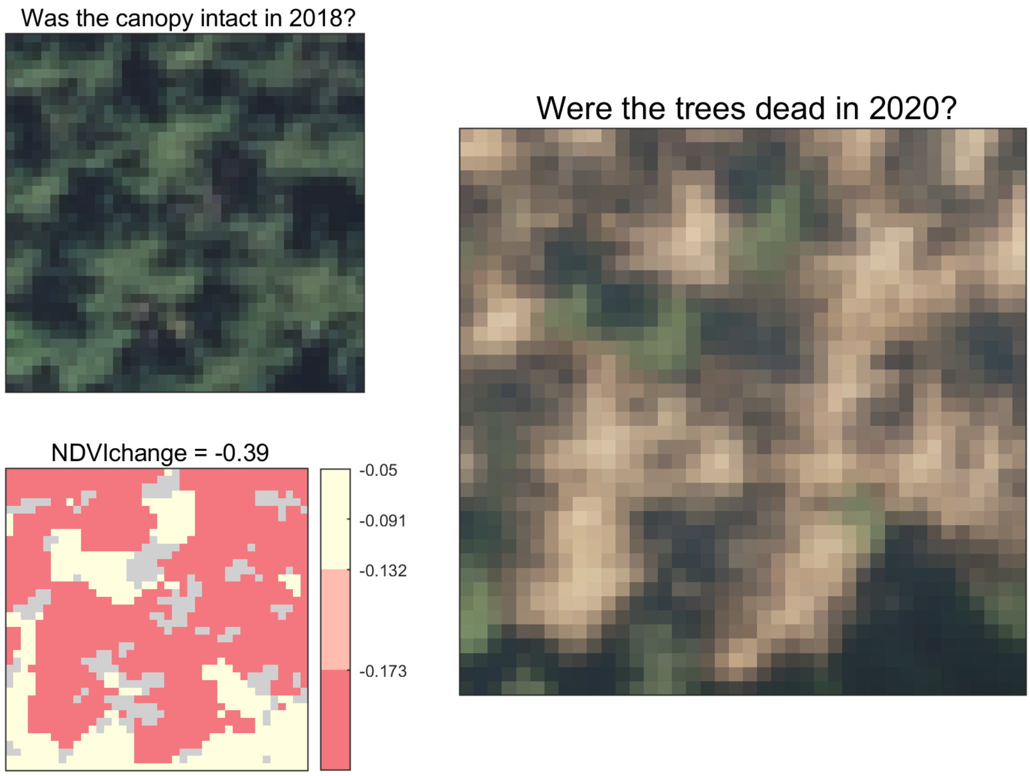

Supplementary Figure S8: Graphical representation of a pre-selected pixel as displayed for optical selection. The pixel shown here was classified as 'damaged' in pre-selection and the optical selection processes. The requirements for the classification were an intact canopy in 2018 and evident damage to the canopy in 2020. Furthermore, the same section should be identifiable and recognizable without, for example, overly large shadows.

proximity. Additionally, the canopy should be visible, with no large-area shadow effects or similar in either year. Based on these criteria, we selected 150 damaged and 121 intact pixels, which were used to validate the 2020 drought resilience. We validated using a standard confusion matrix with dead pixels classified as having resilience $< 15\%$ and a t-test with continuous resilience values.

From a pre-selection based on NDVI values, groups of damaged and non-damaged ('intact') areas were identified in 2020 compared to 2018. Visually damaged areas showed a different drought response than non-damaged areas. Welch's t-test indicates a significant difference between the groups (Supplementary Figure S9). For damaged pixels, we achieved a user's accuracy of 97.26% and a producer's accuracy of 94.67%. The user's accuracy for intact pixels was 97.87%, and the producer's accuracy was 76.03%. The comparably low producer's accuracy for intact pixels can be explained by the validation dataset, including visible damage. Trees that suffered greatly during the drought might show a reduction in water content and LAI but might not show visible damage in the validation dataset.

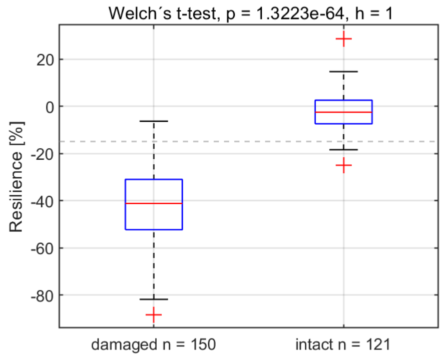

Supplementary Figure S9: Boxplots showing the validation results for the two classes ’damaged’ and ’intact.’

2 Multi-scale analysis

We tested for scale effects using different radii (60 m, 120 m, and 240 m) to derive diversity metrics, resulting in different calculation areas ranging from 1.1 ha to 18.1 ha (see Supplementary Table S5). The three calculation radii were selected as approximations for the calculations in 100 m, 250 m, and 500 m, which were assumed to be relatively large ecosystem scales and landscape scales [5, 6, 7].

Supplementary Figure S10 shows the change in drought response with trait-based diversity at the three different scales of calculation 1.13 ha, 4.5 ha, and 18 ha. Functional richness results in higher values when derived from a larger calculation area, as it is directly affected by the number of data points [8]. Although the value ranges change, the qualitative relationship is constant across the scales. Functional evenness shows a smaller range of values at a large grid. The evenness–resistance relationship shows a less clear hump shape at larger scales, mainly due to the lower value range of low evenness values. Besides these observations, resilience shows a clear relationship with evenness at all calculation scales. However, this relationship is less clear due to the smaller value range and more outliers.

Supplementary Table S5: The three different calculation radii and resulting area.

Radius	60 m	120 m	240 m
# Pixels	28.3 p	113.1 p	452.39 p
Area	1.131 ha	4.524 ha	18.096 ha

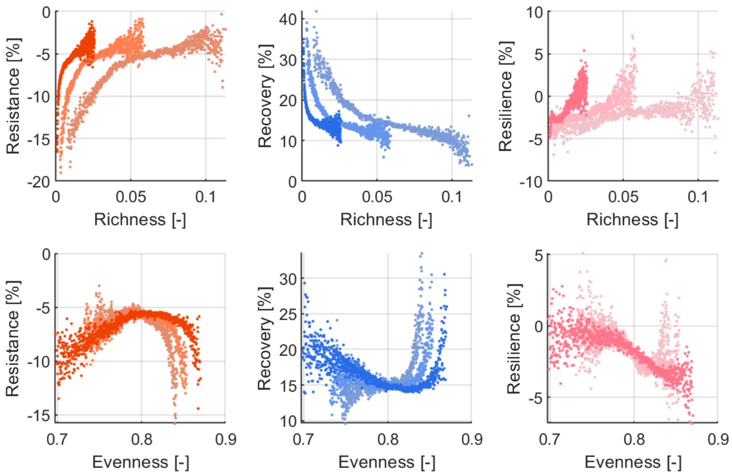

Supplementary Figure S10: Change in RST, RCV, and RSL by quantiles of functional richness (top) and functional evenness (bottom) defined classes with absolute mean values of respective class and by calculation area (1.1 ha – 4.5 ha, dark to light color). The values of diversity ranking (mean per bin) are sorted from low to high.

References

[1] Brändli, K., Stillhard, J., Hobi, M. & Brang, P. Waldinventur 2017 im Naturerlebnispark Sihlwald. *WSL Berichte* **93**, 52 (2020). URL https://www.dora.lib4ri.ch/wsl/islandora/object/wsl%3A23695/datastream/PDF/Br%C3%A4ndli-2020-Waldinventur_2017_im_Naturerlebnispark_Sihlwald-%28published_version%29.pdf.

[2] Zürich. Waldbestandesaufnahme Sihlwald 1990 (1990). URL https://www.parcs.ch/wpz/mmd_fullentry.php?docu_id=9075.

[3] GIS-ZH. Orthofoto Sommer RGB/Infrarot 2018 (OGD) (2018). URL https://www.geolion.zh.ch/geodatensatz/show?gdsid=493.

[4] GIS-ZH. Orthofoto Sommer RGB/Infrarot 2020 (OGD) (2020). URL https://www.geolion.zh.ch/geodatensatz/show?gdsid=527.

[5] Oehri, J., Schmid, B., Schaepman-Strub, G. & Niklaus, P. A. Terrestrial land-cover type richness is positively linked to landscape-level functioning. *Nature Communications* **11**, 1–10 (2020).

[6] Zhang, H. *et al.* Using functional trait diversity patterns to disentangle the scale-dependent ecological processes in a subtropical forest. *Functional Ecology* **32**, 1379–1389 (2018).

[7] Zheng, Z. *et al.* Remotely sensed functional diversity and its association with productivity in a subtropical forest. *Remote Sensing of Environment* **290**, 113530 (2023).

[8] Karadimou, E. K., Kallimanis, A. S., Tsiripidis, I. & Dimopoulos, P. Functional diversity exhibits a diverse relationship with area, even a decreasing one. *Scientific Reports* **6**, 35420 (2016). URL http://www.nature.com/articles/srep35420.